

# Leveraging rapid parameter estimates for efficient gravitational-wave Bayesian inference via posterior repartitioning

Metha Prathaban\*

*Kavli Institute for Cosmology, Madingley Road, Cambridge CB3 0HA, UK and  
Cavendish Laboratory, J.J. Thomson Avenue, Cambridge CB3 0HE, UK*

Charlie Hoy and Michael J. Williams

*Institute of Cosmology and Gravitation, University of Portsmouth, Portsmouth, PO1 3FX, UK*

(Dated: January 30, 2026)

Gravitational wave astronomy typically relies on rigorous, computationally expensive Bayesian analyses. Several methods have been developed to perform rapid Bayesian inference, but they are not yet used to inform our full analyses. We present a novel approach for doing this whilst ensuring that the Bayesian prior remains independent of the data, providing a statistically rigorous way to leverage low-latency information to accelerate the final inference. By combining the fast constraints from the `simple-pe` algorithm with the nested sampling acceleration technique of posterior repartitioning, we demonstrate that our method can guide the nested sampler towards the most probable regions of parameter space more efficiently for signal-to-noise ratios (SNR) greater than 20, while mathematically guaranteeing that the final inference is identical to that of a standard, uninformed analysis. We validate the method through an injection study, demonstrating that it produces statistically robust and unbiased results, whilst providing speedups of up to  $2.2\times$  for binaries with SNRs  $< 150$ . Importantly, we show that the performance gain provided by our method scales with SNR, establishing it as a powerful technique to mitigate the cost of analysing signals from current and future gravitational-wave observatories.

## I. INTRODUCTION

A crucial part of gravitational-wave data analysis is parameter estimation (PE), the process of inferring physical properties of a source, such as its component masses or sky location, from the observed signal, given a model [1]. The results of PE are fundamental to our understanding of stellar evolution, general relativity, and cosmology (most recently, see e.g. [2–10]). As the global network of GW observatories improves in sensitivity and detects an ever-increasing number of events, the demand for efficient analysis methods is growing [11–16], and will become more pressing as more GW detectors come online [17]. This has led to several recent efforts in this area [18–25], including using machine learning algorithms [26–31]. This new era of high signal-to-noise (SNR) signals is exemplified by the recent loud event GW250114\_082203, which, with an estimated network SNR of  $\sim 80$ , is significantly louder than previous detections and promises a new frontier for precision science [32, 33].

The standard approach to perform GW parameter estimation is through Bayesian inference [34, 35]. This is typically accomplished using stochastic sampling algorithms like nested sampling (NS) [36, 37] (although see e.g. Refs. [18, 22] for alternative techniques). Nested sampling is highly effective and reliable, providing not only estimates for the posterior distribution but also the Bayesian evidence required for model comparison [38].

However, the algorithm’s computational cost presents a significant bottleneck. A standard PE analysis for a single event can require millions of likelihood evaluations, often translating to hours or days of runtime on high-performance computing clusters [39]. This computational demand poses an impending challenge for the higher event rates of future observing runs, and already makes the routine use of the most physically comprehensive models, such as those including orbital eccentricity, expensive.

To address the growing computational challenge associated with nested sampling, we introduce a method that combines two existing techniques: posterior repartitioning (PR) [40, 41] and the `simple-pe` analysis [42]. PR is a technique that can accelerate NS by using an approximate posterior, learned from a preliminary NS analysis, to define a more efficient sampling prior [43]. `simple-pe` leverages intuitive physical arguments to produce fast, probabilistic constraints on the source parameters [42], including general relativistic effects such as spin-induced orbital precession [44] and higher order multipole moments [45, 46]. Designed to produce initial parameter estimates in minutes on a single CPU, `simple-pe` can be employed for real-time alerts, as well as for informing more detailed parameter estimation offline.

In this work, we propose a new framework that replaces the preliminary NS run previously used for PR with the rapid, physically-motivated constraints from `simple-pe`. This integration has the potential to be faster and more robust than previous implementations, as it avoids a potentially slow and unreliable preliminary stochastic search. The result is a parameter estimation

---

\* myp23@cam.ac.uk

framework that significantly reduces the number of likelihood evaluations required for convergence, enabling more efficient analysis of both current and future data. Combining our method with techniques that accelerate the single likelihood evaluation time would further improve the performance gains [47–50].

This paper presents and validates this new PE framework. First, we perform a study to characterise how the method’s performance scales with network SNR. This establishes the efficiency gains that can be expected, particularly for the loud events that will become more common in future observing runs. Second, we conduct a large-scale injection study on a population of signals representative of current detections to validate the statistical integrity of the method. We show that it produces unbiased posteriors that are consistent with those from standard NS analyses.

The remainder of this paper is organised as follows. After a review of Bayesian inference and nested sampling in Section II, we detail our PE framework in Section III. We then present two distinct studies to assess the method. In Section IV, we characterise its performance scaling with SNR, and in Section V, we validate its statistical integrity. Both sections detail the study design and present the corresponding results. Finally, we present conclusions and discuss future work in Section VI.

## II. BACKGROUND

### A. Bayesian Parameter Estimation in Gravitational Wave Astronomy

The Bayesian analysis of GW signals involves determining the properties of the astrophysical source, described by a set of parameters  $\theta$ , given the observed strain data  $\mathbf{d}$ . Within the Bayesian inference framework, this is achieved by computing the posterior probability distribution,  $\mathcal{P}(\theta|d, \mathfrak{M})$ , which represents probability of the parameters given the data and a particular underlying model,  $\mathfrak{M}$  [34]. According to Bayes’ theorem, the posterior is given by:

$$\mathcal{P}(\theta|d, \mathfrak{M}) = \frac{\pi(\theta|\mathfrak{M})\mathcal{L}(d|\theta, \mathfrak{M})}{\mathcal{Z}(d|\mathfrak{M})}. \quad (1)$$

The model remains unchanged throughout this study, so we will omit the explicit dependence on the model but we refer interested readers to e.g. [51–53] for multi-model inference. Here,  $\pi(\theta)$  is the prior probability distribution, encoding our pre-existing knowledge about the parameters. The term  $\mathcal{L}(d|\theta)$  is the likelihood, which quantifies the probability of observing the data  $d$  given a specific set of parameters. The denominator,  $\mathcal{Z}(d)$ , is the Bayesian evidence, obtained by integrating the product of the likelihood and prior over the entire parameter space:

$$\mathcal{Z}(d) = \int \pi(\theta)\mathcal{L}(d|\theta) d\theta. \quad (2)$$

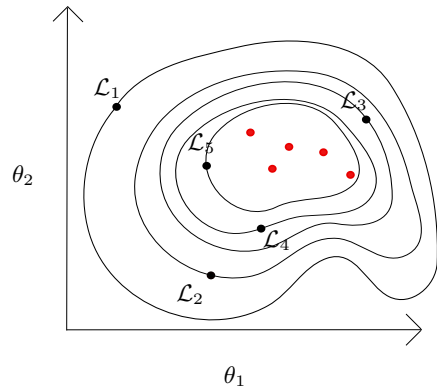


FIG. 1. Cartoon of nested sampling algorithm in two dimensions. Dead points define nested likelihood contours, indicated by  $\mathcal{L}_1, \mathcal{L}_2, \dots$ , in the parameter space, and the live points compress exponentially towards the peak of the likelihood as the algorithm proceeds. The fractional prior volumes enclosed between successive contours determine the weights of each dead point, used for calculating the Bayesian evidence and drawing posterior samples.

While essential for comparing competing models within Bayesian methodology [38] (although this does not account model accuracy, see Refs. [52, 53]), the evidence is computationally expensive to calculate.

### B. Nested Sampling

There exist several stochastic sampling methods to estimate the posterior distributions of GW data, such as MCMC [54, 55] and nested sampling [35, 38, 56–58]. NS is a Monte Carlo algorithm specifically designed to calculate the Bayesian evidence. NS works by drawing a set of ‘live points’ from the prior distribution. At each iteration, the point with the lowest likelihood is removed from the live set, being made a ‘dead point’, and is replaced with a new point drawn from the prior, subject to the constraint that its likelihood must be higher than that of the point it is replacing. This process generates a sequence of live points that iteratively move from the broad prior volume into progressively smaller regions of higher likelihood (see Figure 1). The collection of dead points, when appropriately weighted, provides samples from the posterior, while the sum of their likelihood values multiplied by their enclosed prior volume fractions yields a robust estimate of the evidence.

Despite its effectiveness, NS is computationally intensive. A single analysis often requires hours to days of processing time on high-performance computing clusters (although it has been shown that nested sampling can be parallelised over many CPUs [59], reducing the overall wall time, and techniques have been developed to optimise the GW likelihood [21, 24, 47, 48, 60–65], reducing the overall processing time). This cost is an obstacle to

achieving rapid scientific turnaround for the large event catalogs of current and future observatories; assuming nested sampling continues to be used [13, 66]. For example, it has been shown that a full nested sampling algorithm with the future Laser Interferometer Space Antenna (LISA) observatory can take more than  $10^5$  CPU hours [67].

### III. METHODS

#### A. Posterior Repartitioning

One method to reduce the computational cost of nested sampling is posterior repartitioning, which improves sampling efficiency by exploiting a fundamental property of Bayesian inference [40, 41, 43, 68]. The posterior distribution and Bayesian evidence depend only on the product of the likelihood and the prior,  $\mathcal{L}(\theta)\pi(\theta)$ . We are therefore free to redefine these two components for computational purposes, so long as their product remains invariant.

Nested sampling is uniquely suited to this manipulation because its algorithm explicitly separates the prior and the likelihood, by ‘sampling from the prior subject to a hard likelihood constraint’. PR leverages this by redefining the prior that the NS algorithm sees. The procedure is as follows (also see Figure 2):

1. An approximation to the target posterior,  $g(\theta)$ , is generated. In the past this has been achieved by training a normalizing flow on samples from a preliminary, low-resolution nested sampling run [43]. Normalizing flows learn a series of invertible mappings from a base distribution to a target [69, 70].
2. This learned distribution  $g(\theta)$  is assigned as the new, effective prior for the NS algorithm. This is the **repartitioned prior**,  $\pi'(\theta) \equiv g(\theta)$ .
3. To ensure the likelihood-prior product is unchanged, the likelihood must be redefined with a corrective term:

$$\mathcal{L}'(\theta) = \mathcal{L}(\theta) \left[ \frac{\pi(\theta)}{\pi'(\theta)} \right] \quad (3)$$

The term in the brackets is the repartitioning factor. The nested sampler is then executed using  $\pi'(\theta)$  as its sampling prior and  $\mathcal{L}'(\theta)$  for its likelihood evaluations.

It is important to note that this is purely a computational technique; the true Bayesian prior  $\pi(\theta)$  of the inference problem is not altered. The result is an NS run that converges faster because its sampling is concentrated within the smaller volume of the repartitioned prior, which by design already resembles the posterior. The acceleration from PR fundamentally depends on the quality of the initial approximation,  $\pi'(\theta)$ . The approach

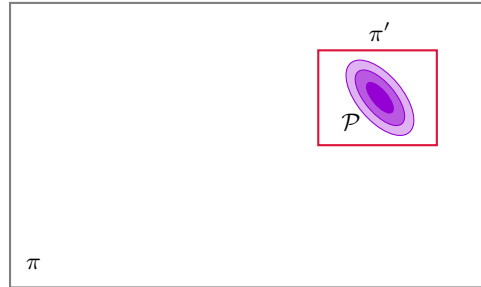


FIG. 2. Most of the computational time of nested sampling is spent in locating the bulk of the posterior,  $\mathcal{P}$ , within the much larger prior volume,  $\pi$ . In posterior repartitioning, this region of interest is first identified by an approximate method. The nested sampling run is then initialised within this smaller volume,  $\pi'$ , using a repartitioned likelihood (Eq. 3) to ensure the resulting posterior and evidence are identical to a standard analysis.

of using a low-resolution NS run for initialisation, as in [43], presents two key drawbacks. First, the preliminary run itself can be computationally expensive, offsetting some of the efficiency gains. Second, and more critically, a stochastic sampler run in a low resolution configuration may fail to identify complex posterior structures, such as sharp peaks or secondary modes. If the initial approximation is poor, posterior repartitioning can be ineffective or, in the worst case, can cut off at the algorithmic level regions of the parameter space with non-negligible posterior probability, leading to biased results. Signals with lower signal-to-noise ratios (SNR) can be particularly susceptible to these issues.

We note that similar techniques that leverage preliminary or intermediate results have been developed for Markov Chain Monte Carlo and Sequential Monte Carlo [71, 72]. We focus on PR, as nested sampling is the current standard for GW analyses. We leave a comparison to other approaches for further work. We also note that acceleration techniques which optimise the GW likelihood are complementary to PR and, whilst not considered, could also be applied.

#### B. simple-pe

The **simple-pe** algorithm provides a rapid analysis framework that generates estimates for the posterior probability distribution within minutes on a single CPU [42]. Instead of performing a full Bayesian analysis with stochastic sampling, **simple-pe** uses simple, intuitive, and physical insights to estimate the source properties.

**simple-pe** takes advantage of the well-known physical decomposition of GW signals, whereby a GW signal can be decomposed into an infinite sum of spin-weighted spherical harmonics [45, 46]. However, **simple-pe** relies on the fact that only a small number of these terms sig-

nificantly affect the observed signal; it can be shown that a GW signal consistent with general relativity (assuming quasi-circular orbits) can be described to high fidelity as a sum of three orthogonal components [42, 73]. In essence, the dominant term describes the base chirp-like signal, the second term describes the contribution due to spin-induced precession and the third term describes the contribution from higher order multipole moments. The central principle of `simple-pe` is that a measurement of the dominant term provides the primary information for the intrinsic parameters: chirp mass, mass ratio, and aligned spins. A measurement of the precessing and/or higher order multipole terms then further constrains these intrinsic measurements and provides information on the extrinsic properties. While `simple-pe` is capable of analysing precessing systems, with the possibility of incorporating eccentric binaries [74], this is not explored in this work.

The `simple-pe` algorithm treats parameters hierarchically. It first identifies the most likely chirp mass, mass ratio and aligned-spin based on the best fitting dominant only-term that maximises the matched filter SNR. It then approximates the likelihood surface around this 3 dimensional peak as a multivariate Gaussian, where the width is based on the expected accuracy at which the mass and spin can be measured, accounting for known degeneracies throughout the parameter space [75]. This simple distribution allows for the rapid generation of initial mass and spin samples. Extrinsic parameters, such as distance and orientation, are handled separately by sampling from constrained distributions that depend on the network SNR and response. Finally, SNRs for features beyond the dominant term are obtained by matched filtering the data again, and these initial samples are refined through a re-weighting step; each sample is assigned a weight based on the probability of obtaining each of the observed SNRs.

While this approach sacrifices the full rigour of an NS analysis, its physically-informed logic makes it a more robust tool for generating initial parameter estimates. Because its constraints are derived from specific physical features rather than stochastic exploration, it may be less susceptible to the same failure modes as a low-resolution sampler. For example, it is potentially less likely to miss secondary modes of the posterior, such as in the inclination angle, which is known to be often bimodal. This makes it an ideal candidate for improving the initialisation stage of posterior repartitioning.

However, due to the approximations employed, `simple-pe` in its current form may not guarantee the most reliable estimates. For example, for binaries with significant spin-precession or higher order multipoles, more than three terms are needed in the waveform expansion to fully describe the observed signal [76, 77]. By neglecting some higher order multipole power, biases may be expected particularly in high mass systems (see e.g. [78]). Similarly, by using only the dominant term to initially provide samples for the mass and spin of the bi-

nary, biases may be expected for high SNR signals with significant contributions from subdominant terms [73] (although the initial samples are re-weighted to account for the observed power in subdominant terms; if the initial distribution lies outside of the region consistent with the observed power, the re-weighting procedure fails). Finally, `simple-pe` may struggle for low SNR signals since the multivariate Gaussian approximation for the initial mass and spin samples begins to break down.

### C. The `simple-pe-PR` Algorithm

Our method integrates the constraints from `simple-pe` into the posterior repartitioning framework through a multi-step algorithm. The full procedure, shown schematically in Fig. 3, is as follows:

- 1. Initial Constraints:** The method begins by running `simple-pe` on the gravitational-wave strain data to generate a set of samples. These samples provide a rapid, physically-motivated initial approximation of the posterior.
- 2. Learning a Continuous Distribution:** The discrete samples from `simple-pe` must be converted into a continuous probability distribution from which we can both sample and evaluate the log-probability. We achieve this by training a normalizing flow, using a modified version of the `margarine` software [79–81], on the `simple-pe` samples (see Appendix B for details). This flow serves as a learned, continuous representation of the initial posterior approximation. However, other methods besides normalizing flows are possible for obtaining this, such as generation of a multi-dimensional kernel density estimate [82], or Gaussian processes [83].
- 3. Widening for Robustness:** Due to the approximations employed, the distribution produced by `simple-pe` can be narrower than, or offset from, the true posterior [84]. To prevent this from biasing the final inference, the learned distribution is widened. The specific widening factors applied are an important choice, and their empirical calibration based on our injection study is detailed in Section V. The widening itself is achieved by modifying the base distribution of the trained normalizing flow. Specifically, we increase the standard deviation of the base multivariate Gaussian distribution. The covariance matrix is diagonal, meaning that we can change the standard deviation for each dimension independently. 2000 samples are then drawn from this ‘widened’ flow. A second normalizing flow is then trained on these widened samples to produce the final, robust repartitioned prior,  $\pi'(\theta)$ . During training of both flows, we do

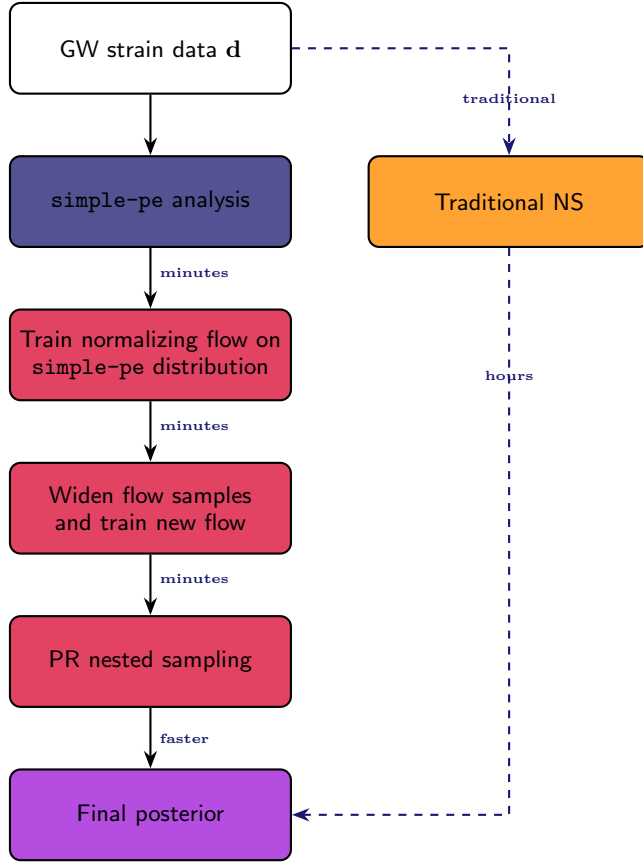


FIG. 3. A flowchart of our proposed algorithm. Our method (left) introduces several fast pre-processing steps before running a posterior repartitioned (PR) nested sampling analysis. This reduces the runtime compared to a traditional nested sampling (NS) analysis (right). The primary computational bottleneck in both methods is the nested sampling step itself. Provided the initial `simple-pe` distribution is sufficiently widened, our method produces the same posteriors as the traditional approach but with significantly fewer likelihood evaluations.

not apply bounds and allow the flows to have support outside the original prior. This will not affect the final inference as samples outside the original prior will not be accepted by the sampler anyway, and we discuss this further in Appendix B.

**4. Final Parameter Estimation:** The final PE analysis is performed using `bilby-pr`, a custom, pip-installable `bilby` plugin package developed for this work [85]. This package extends the standard `dynesty` sampler [57] as implemented in `bilby` [56], with arguments to accept a pre-trained `margarine` normalizing flow. It then implements custom prior and likelihood wrappers that employ the flow as the new repartitioned prior,  $\pi'(\theta)$ , and adjust the likelihood according to Eq. 3.

The repartitioned prior,  $\pi'(\theta)$ , does not incorporate information for all parameters. The constraints from

Parameter	Value
Chirp mass ( $\mathcal{M}_c$ )	$22.5 M_{\odot}$
Mass ratio ( $q$ )	0.11
Right ascension ( $\alpha$ )	1.11 rad
Declination ( $\delta$ )	1.33 rad
Inclination angle ( $\theta_{\text{JN}}$ )	2.59 rad
Polarization angle ( $\psi$ )	1.01 rad
Phase at coalescence ( $\phi$ )	3.82 rad
Spin of lighter BH ( $\chi_1$ )	0.28
Spin of heavier BH ( $\chi_2$ )	0.49
Time of coalescence ( $t_c$ )	1367638517.66 s

TABLE I. Fiducial detector frame parameters for the injection used in the SNR scaling study. The luminosity distance is not listed as it was varied to achieve the target SNRs.

`simple-pe` on the sky location parameters, right ascension ( $\alpha$ ) and declination ( $\delta$ ), exhibited a variance in accuracy that made them unsuitable for reliable repartitioning [86]. Similarly, `simple-pe` does not provide distributions for the phase, polarization angle, and time of coalescence. For these parameters, we retain the original priors. Finally, since we analytically marginalise over luminosity distance in the likelihood in order to improve convergence [87, 88], we do not use the `simple-pe` distance estimates. In summary, our repartitioned prior only incorporates information from `simple-pe` for the intrinsic binary parameters and the inclination angle, where its performance is most robust.

#### IV. SNR SCALING STUDY

As described, the efficiency of posterior repartitioning is determined by the quality of the initial posterior approximation. Since both the precision of `simple-pe` and the concentration of the true posterior are expected to improve at higher SNR, we anticipate that the computational speedup of the `simple-pe-PR` algorithm will grow with signal strength. We therefore first conduct a targeted study to investigate the performance of our method for signals with varying SNR.

We focus on a single fiducial binary black hole merger. The parameters for this injection are listed in Table I, and were chosen randomly from the prior specified in Table III. We then generated a series of signals, each 8 seconds in duration. For each signal, all source parameters were held constant except for the luminosity distance, which was scaled to produce signals with target network SNRs of 10, 20, 30, 40, 50, 75, 100, and 150.

The signals were generated using the aligned-spin waveform model `IMRPhenomXHM`, which includes higher order multipoles [89]. They were injected into coloured Gaussian noise representative of the design sensitivity of the Advanced LIGO-Hanford (H1), LIGO-Livingston (L1), and Virgo (V1) detectors [90]. For each of the signals, we performed two analyses: one using a standard nested sampling algorithm and one using the

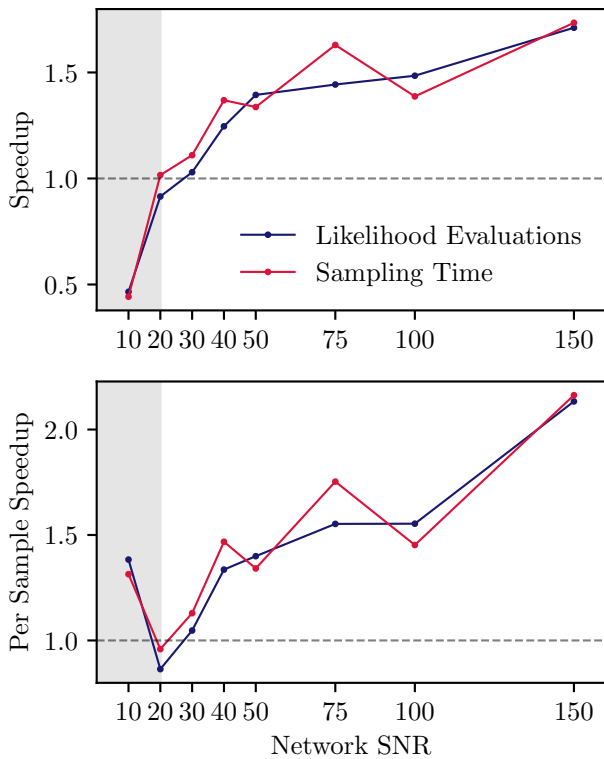


FIG. 4. Performance of the `simple-pe-PR` method relative to a standard nested sampling analysis as a function of network SNR. The speedup factor is the ratio of a metric for the standard analysis to that of the PR analysis. *Top*: Total speedup factors, showing the ratio of total likelihood evaluations (blue) and total sampling time (crimson). *Bottom*: Speedup factors normalised by the number of effective posterior samples. The dashed line at 1.0 indicates no change in performance. The shaded and non-shaded regions separate the two different regimes used for the widening factors.

`simple-pe-PR` algorithm described in Section III C. For the `simple-pe-PR` analyses, we applied the appropriate SNR-dependent widening factors as determined in the injection study (see Section V and Table II).

For both analyses, the nested sampling step was performed with the `dynesty` sampler [57] as implemented in `bilby`. We used the priors detailed in Table III in Appendix A, but adopted a wider luminosity distance prior, from 100 to 5000 Mpc, which was more suitable for the low-SNR injections in this study. The right ascension ( $\alpha$ ), polarization angle ( $\psi$ ), and phase at coalescence ( $\phi$ ) were treated with periodic boundary conditions. Identical sampler settings were used for both the standard and PR analyses to ensure a direct comparison. The key sampler settings were: `nlive` = 1000, `sample` = ‘acceptance walk’, `naccept` = 60, `maxmcmc` = 5000, and `use_ratio` = `True` [1].

For all signals in this study above SNR 20, the posterior distributions produced by both methods were compared and found to show excellent agreement across all

one- and two-dimensional marginal distributions (see e.g. Figure 8, or [91] for the posterior files). Moreover, we calculated the Jensen-Shannon divergence (JSD) between each set of samples at a given SNR and found that all values are within the threshold for  $\text{SNR} > 10$  (see Appendix D for further details).

For the SNR 10 signal, our `simple-pe-PR` method produced a narrower posterior on the mass ratio,  $q$ , than standard NS. This is because the widening of the initial `simple-pe` distribution was insufficient to cover the full posterior. This is a known failure mode of the method at  $\text{SNR} \leq 10$ , as discussed in V. For the SNR 20 signal, the standard NS analysis revealed a small secondary mode in the inclination angle (containing 0.6% of the samples) that was absent from our method’s result. This feature was not present in the initial `simple-pe` estimate and was sufficiently distant from the primary mode that our widening procedure did not fully encompass it (see Figure 5). This exemplifies another limitation of the method: the efficiency gained from a focused initial guess comes with a risk of missing isolated, low probability posterior features that lie far outside that approximation. This risk is most pronounced at low SNRs where posteriors can be complex, and is significantly mitigated for high SNR signals, where `simple-pe` is known to perform better and where the posteriors are less likely to be multimodal. Moreover, `simple-pe` produces samples drawn from a weighted distribution. This means that the risk can be further mitigated even at lower SNRs by drawing more samples, which takes negligible additional time, to include sufficient samples from the secondary mode in the training set for the normalizing flow. Alternatively, the flow could also be trained directly on the weighted samples themselves. However, given the expected computational speedups (see below), we recommend anyway the application of our method to signals with  $\text{SNR} > 20$ .

We quantify the performance improvement, or speedup, of our method as the ratio of a given metric (e.g., number of likelihood evaluations) for a standard NS analysis to that of our `simple-pe-PR` analysis. The total runtime of our method is dominated by the nested sampling step. `simple-pe` took on average 5 minutes on a single CPU per injection, and training both the original and widened normalizing flows together took under a minute on average on a single CPU. For comparison, the nested sampling step took on average 7 hours, parallelised over 38 CPU cores. Therefore, when comparing runtimes, we only consider the respective nested sampling times of each method.

The overall speedup factors as a function of optimal network SNR are shown in the top panel of Fig. 4. At SNR 10 and 20, our method is slower than the standard approach. At SNR 10, this behavior is a consequence of the posterior distribution itself being broader at low SNR. The runtime of nested sampling is related to the Kullback-Leibler (KL) divergence between the prior and the posterior, which can be thought of as the ‘amount of compression’ required for the sampler to con-

verge [38, 43, 68]. For a low-SNR signal, this divergence is modest, and the standard NS analysis already converges relatively quickly. In this regime, applying a conservative widening factor to the already broad **simple-pe** approximation can create a repartitioned prior,  $\pi'(\theta)$ , that is a poorer representation of the posterior than the original prior,  $\pi(\theta)$ . This can increase the effective KL divergence, leading to a longer runtime (see Appendix C for further discussion). Additional sampling inefficiencies can also be introduced if the widened flow proposes samples outside the support of the original prior (see Appendix B for further discussion). It is possible that a more automated widening procedure or a limit on how much wider the **simple-pe** informed prior can be relative to the original prior would mean that our **simple-pe**-PR method would achieve comparable runtimes. We discuss this later in Section V.

At SNR 20, the repartitioned prior is a better representation of the final posterior than the original prior (see Appendix C). However, in this case the missed secondary mode in the widened flow leads to sampling inefficiencies. The sampler attempts to explore the part of the parameter space containing the secondary mode, recognising it as a region of high likelihood for the repartitioned analysis (Eq. 3), but since this lies deep in the tails of the widened flow, the analysis requires more likelihood evaluations (Figure 5).

As the SNR increases, however, the method’s performance improves substantially. Above SNR 20, **simple-pe**-PR becomes more efficient than standard NS. Although many of the signals in version 4.0 of the Gravitational-Wave Transient Catalog (GWTC-4.0) have SNRs  $< 20$ , 6% have SNRs  $> 20$  [92], and this percentage is likely to increase as detector sensitivity improves [13]. At SNR 150, the number of likelihood evaluations and the total sampling time are reduced by a factor of 1.7, corresponding to a 41% reduction in runtime. The difference between these two metrics at different SNRs arises from the computational overhead of the repartitioned likelihood (Eq. 3). This calculation requires evaluating not only the original likelihood, but also the log-probabilities of both the normalizing flow and the original prior. This additional cost would be mitigated if a vectorised sampler were used, which could evaluate the flow probabilities of multiple points at once, reducing the average single particle evaluation time [22, 58, 93–96]. While the overall trend shows a clear monotonic increase in performance with SNR, minor deviations in the sampling time are consistent with temporal variations in CPU node performance on high performance computing systems. Although SNR 150 signals are unlikely to be routinely observed until the advent of third-generation (3G) detectors or LISA [97–101], our method still provides an improvement on standard NS above SNR 20; we already see speedups of above 1.5 at SNR  $> 50$ , a regime where signals are starting to be observed in O4 and will become more frequent in O5.

For a more detailed comparison, the bottom panel of

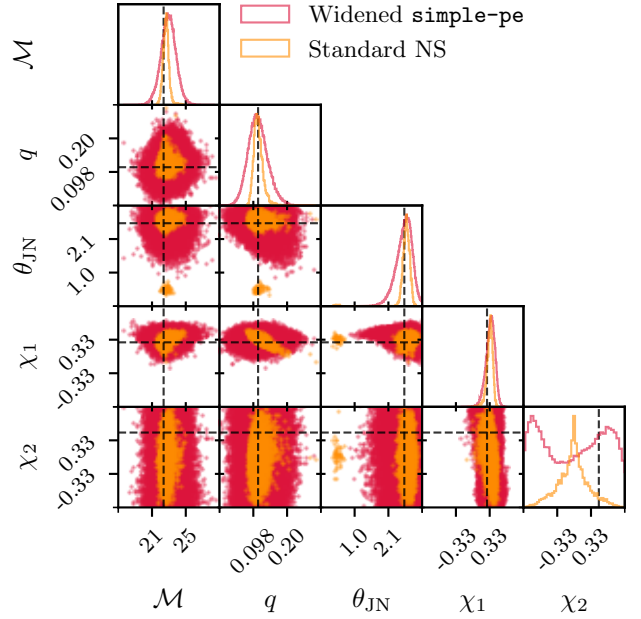


FIG. 5. For the SNR 20 signal, **simple-pe** did not produce sufficient samples from the secondary mode of the true posterior in order for the flow to learn this feature. The widened flow is able to generate samples which lie in this secondary mode, but with very low probability. Since the sampler recognises that this region of the parameter space has a high repartitioned likelihood, it attempts to explore it, but inefficiently and unsuccessfully, leading a marginally slower analysis than standard NS and a slightly different final posterior. This issue can be mitigated by drawing more initial samples from **simple-pe** to make sure the secondary mode is sufficiently covered.

Fig. 4 shows the speedup factor normalised by the number of effective posterior samples produced by each analysis (calculated as in [102]). The PR analysis typically spends a larger fraction of its runtime sampling the high-likelihood region of the parameter space, often yielding a larger number of effective samples than a standard analysis with the same settings (see Appendix E). When this is accounted for, the performance at low SNR is more favourable; only the SNR 20 analysis is marginally slower. At SNR 150, the number of likelihood evaluations and total sampling time are now reduced by a factor of 2.1 (a 53% reduction in the runtime). Due to PR typically populating the bulk of the posterior more densely, our method can be performed with fewer live points than a standard NS analysis for the same final sample size and resolution. As such, the per-sample speedup can be interpreted as the more informative performance metric as it compares like-for-like inference products. Furthermore, the per-sample speedup at high SNR shows no sign of saturating, suggesting that further efficiency gains may be possible for even louder signals, such as those from 3G detectors or LISA [103].

The origin of this speedup is illustrated in Fig. 6. As

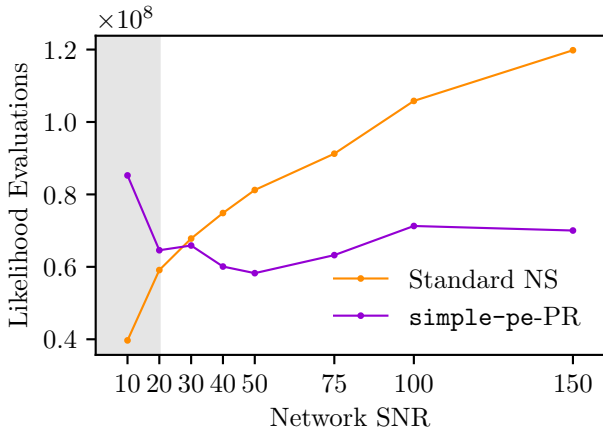


FIG. 6. Total number of likelihood evaluations as a function of network SNR for a standard analysis (orange) and our **simple-pe-PR** analysis (violet). The computational cost of the standard analysis grows with SNR, while the cost of the PR analysis remains approximately constant for  $\text{SNR} > 20$ .

expected, the number of likelihood evaluations required by the standard NS analysis grows with SNR. This is because the posterior volume becomes increasingly small relative to the prior, increasing the number of iterations of the algorithm required for convergence. In contrast, the number of likelihood evaluations for the PR analysis shows no strong scaling with SNR for signals above SNR 20, remaining approximately constant within the stochastic variations expected from the normalizing flow training and the sampling process. Our method effectively removes the expensive initial ‘search phase’ of the nested sampling algorithm (see Figure 7).

This efficiency gain has significant practical implications. As well as reducing runtimes by hours to days, this reduction in cost lowers the barrier for performing analyses with more physically complete but expensive waveform models, such as those including orbital eccentricity [104–107].

## V. INJECTIONS

Having characterised the performance of **simple-pe-PR** with scaling SNR, we now conduct a large-scale injection study to validate its statistical integrity across a broad range of binary properties. The primary goal of this study is to demonstrate that our method produces the expected range of distributions from a Gaussian likelihood in noise, consistent with the standard version of `bilby` and nested sampling [108].

We performed the injection study using 100 simulated binary black hole merger signals, each 8 seconds in duration. The parameters for these injections were drawn from the prior distributions detailed in Table III in Appendix A. This choice of priors is representative of those

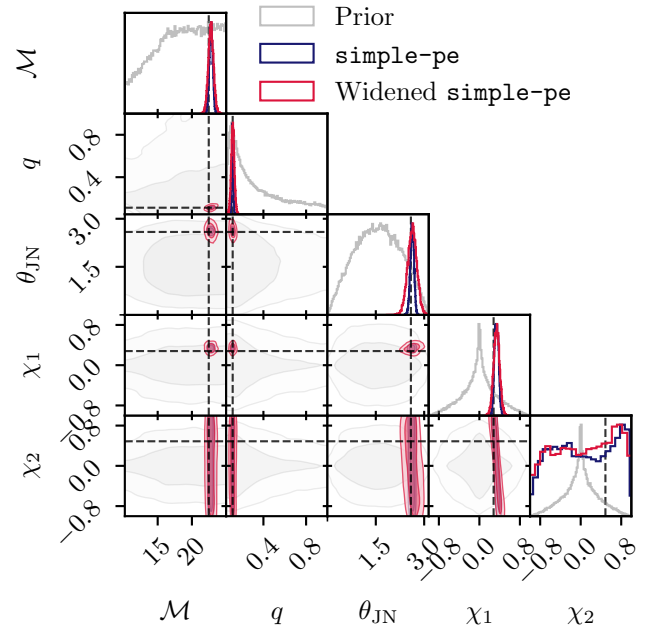


FIG. 7. The prior,  $\pi$ , **simple-pe** distribution and widened distribution used as the repartitioned prior,  $\pi'$ , are shown for the SNR 40 injection. The repartitioned prior occupies a much smaller volume than the original prior, reducing the number of likelihood evaluations required for convergence. In all parameters but the spin of the heavier BH ( $\chi_2$ ), the repartitioned prior is much more constrained than the original prior and effectively removes the initial ‘search phase’ of NS.

used in LVK analyses, including the choice of mass priors (see Appendix A for further discussion). It therefore allows us to validate our method’s statistical robustness in this same parameter range.

The injection and recovery of each signal followed the procedure detailed in Section IV. The signals were generated with the `IMRPhenomXHM` waveform model and injected into coloured Gaussian noise. Each signal was then analysed with both standard NS and our **simple-pe-PR** method, using identical sampler settings.

A key component of our method is the widening of the initial **simple-pe** distribution to ensure the resulting posteriors are unbiased. We used this injection study to perform an empirical calibration of the necessary widening factors. For each of the 100 signals, we compared the initial **simple-pe** distribution to the full posterior from the standard NS analysis. We then determined the widening factor for each repartitioned parameter required to ensure the 1st and 99th percentiles of the standard posterior were contained within the 1st and 99th percentiles of the widened distribution.

This calibration confirmed that the performance of **simple-pe** depends on the network SNR [42]. A notable change in behavior was observed around an SNR of 20. Consequently, we adopted two distinct sets of widening factors: one for signals in the lower-SNR regime ( $10 \leq$

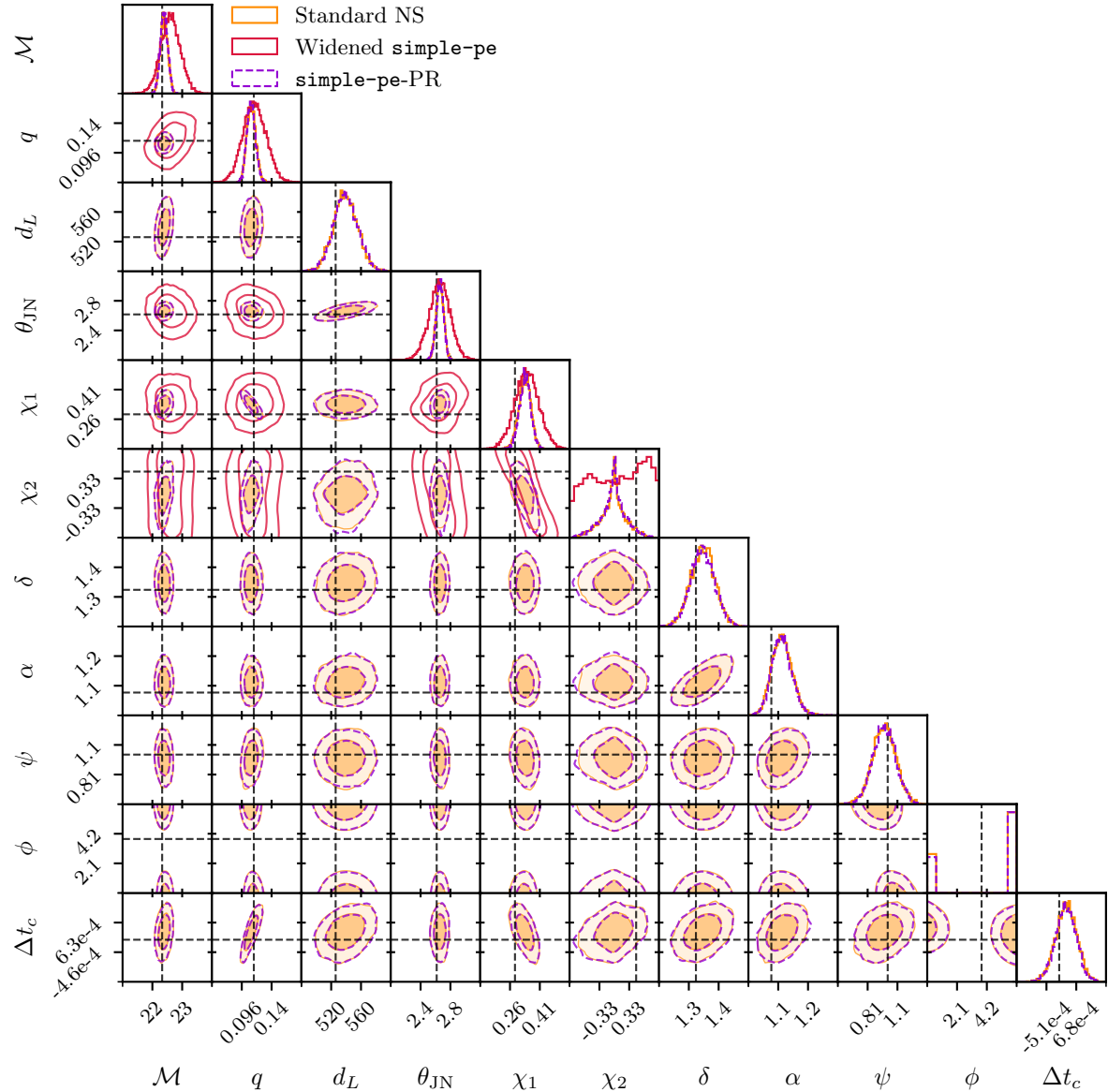


FIG. 8. Validation of the `simple-pe-PR` method on the SNR 40 injection. The one- and two-dimensional marginal posterior distributions from our method (violet) are plotted alongside those from a standard NS analysis (orange), showing excellent agreement. The repartitioned prior,  $\pi'$ , used to accelerate the analysis is also shown for the five parameters to which it was applied (crimson).

network SNR  $< 20$ ) and a less conservative set for high-SNR signals (network SNR  $\geq 20$ ), shown in Table II. For signals below SNR 10, the required widening becomes large enough to negate any computational benefit from posterior repartitioning. While we apply the lower-SNR factors to these signals for the purpose of our injection study, this fixed widening is often insufficient to guarantee an unbiased posterior, reinforcing our recommendation against applying the method in this regime.

Finally, we note that these widening factors were calibrated on aligned-spin injections in a three-detector network. They may vary for analyses involving two-detector

Parameter	Widening Factor ( $w$ )
Mass Ratio ( $q$ )	2.5
Chirp Mass ( $\mathcal{M}_c$ )	2.0 (1.5)
Spin of lighter BH ( $\chi_1$ )	2.0 (1.5)
Spin of heavier BH ( $\chi_2$ )	1.0
Inclination angle ( $\theta_{\text{JN}}$ )	2.5

TABLE II. Widening factors ( $w$ ) applied to the standard deviation of the normalizing flow's base distribution for signals with network SNR  $< 20$  (SNR  $\geq 20$ ).

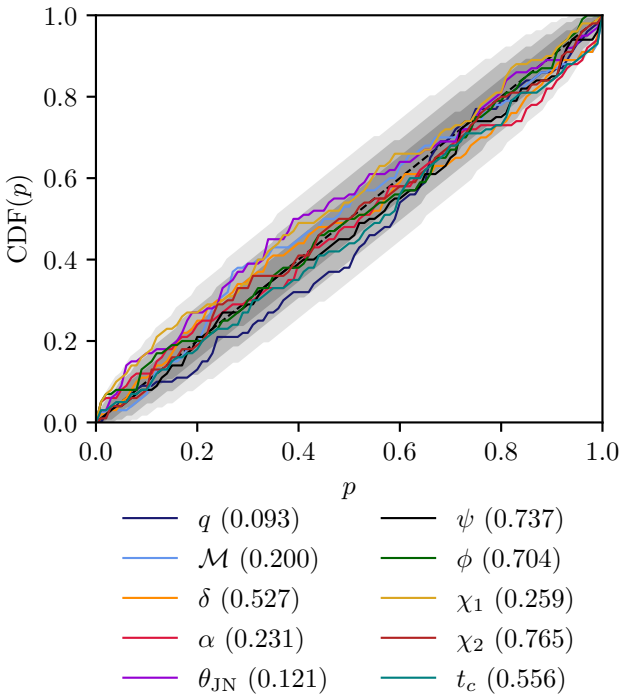


FIG. 9. Probability-probability (P-P) plot for the 100 injections in our validation study. Each coloured line represents the cumulative distribution function (CDF) of the posterior quantiles of the true injected values for a specific parameter. The diagonal dashed line represents a perfect uniform distribution, while the shaded gray regions indicate the  $1\sigma$ ,  $2\sigma$  and  $3\sigma$  confidence intervals. The p-values from a Kolmogorov-Smirnov test for each parameter are shown in the legend. The combined p-value is 0.3342.

networks or precessing binary systems. While this widening process could be automated in future work, using techniques similar to those introduced in [43], we do not explore this here.

The statistical integrity of our method is validated using a probability-probability (P-P) plot (Figure 9), used for identifying biases in inferred posterior distributions [109]. A P-P plot shows the fraction of signals for which the injected parameter values lie within a given credible interval, as a function of the credible interval. In the ideal case where the parameter inference procedure leads to the correct coverage, this plot should be a diagonal line. However, there is a statistical uncertainty that arises from the finite number,  $N$ , of signals analysed, indicated by the gray regions in Figure 9. The recovered distributions for all parameters from our method are consistent with unbiased posterior distributions within this statistical uncertainty. The distribution of credible intervals for the true injection parameters is consistent with a uniform distribution, and the p-values from a Kolmogorov-Smirnov (KS) test for each parameter are all greater than 0.05. Moreover, they are similar to the equivalent p-values obtained from standard NS (see Ap-

pendix F for this P-P plot). We quantify the agreement between the two P-P plots by performing a two-sample KS test, comparing the respective distributions of percentiles, and find that for all parameters the p-values are greater than 0.9. This demonstrates that on a population level the posteriors are statistically consistent.

We also compute the individual one-dimensional JSD values between the two sets of posterior distributions for each injection (see Appendix D). For the majority of injections, the posteriors from `simple-pe-PR` are in good agreement with those from standard NS, confirming the general robustness of the widening procedure. Nevertheless, we observed two injections above SNR 20 that exhibited significant differences in the posterior estimates. In both cases, this was because the `simple-pe` estimate of the inclination angle was severely offset from the nested sampling posterior, due to `simple-pe` identifying the opposite sky mode. Our widening procedure is not designed to account for such cases where the initial estimate is significantly separated from the posterior. This type of failure, where a significant offset in the initial `simple-pe` guess leads to posterior disagreement, occurs more frequently at lower signal strengths. Between SNR 10 and 20, five injections, representing approximately 10% of signals in this range, show significant posterior differences. Below SNR 10, this number increases to 9 of the 14 injections, an expected result as our widening factors were not calibrated for this regime.

Although the inclination angle failure mode can produce biased posteriors in rare instances, we still include it in our repartitioned prior to leverage the noticeable speedups it provides for the majority of signals. The risk associated with cases where the initial `simple-pe` approximation lacks sufficient fidelity is a known limitation of the current fixed-widening scheme. Further improvements to the `simple-pe` algorithm will alleviate this, not only ensuring more robust results at all signal strengths, but also reducing the need for our widening procedure. Moreover, the widening procedure itself could be improved by varying the degree of widening on the fly during the analysis, by sampling over an additional widening factor parameter. This would enable larger widening factors to be incorporated for more challenging signals without sacrificing performance on signals which require little to no widening (see below).

Figure 10 shows the per-sample speedup factor for each injection as a function of network SNR. As anticipated by the scaling study, there is a clear positive trend in performance with SNR, albeit with significant scatter. The maximum speedup observed is 2.2, for an injection with SNR 46. This performance distribution reflects the characteristics of our injection set, which was drawn from the prior distributions used in LVK analyses. However, the prior on the luminosity distance was narrowed to ensure that most of the resulting signals have SNRs that are detectable (Table III). Even so, the majority of signals have network SNRs below 20 (shaded region), the regime where the performance of our method is expected

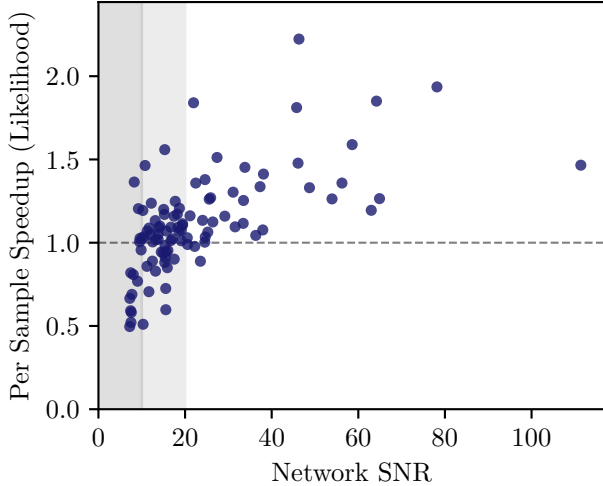


FIG. 10. Per-sample likelihood evaluation speedup factor for each of the 100 injections, as a function of network SNR. Each point represents a single analysis. The lighter shaded region ( $\text{SNR} < 20$ ) highlights the regime where the speedup is unreliable. It also marks the boundary of the two sets of SNR-dependent widening factors. The darker shaded region indicates where the calibrated widening factors may not be large enough to obtain unbiased results. The dashed line at 1.0 indicates no change in performance relative to a standard analysis.

to be modest, or in some cases worse than standard NS. We find that 74% of injections in our population show speedups greater than 1, and for signals with  $\text{SNR} > 10$ , this figure increases to 81%.

The widening factors we use are intentionally conservative to ensure robustness for the majority of signals with SNRs above 10. For many signals, the initial distributions require little to no widening; 25% of the injections needed widening factors less than 1.25 in all parameters. As discussed in Section IV, this has an impact on the observed performance gains. Separately, for signals below  $\text{SNR} 10$ , the widening procedure is not guaranteed to be sufficient to produce unbiased estimates for the posterior for all individual cases, as explained above.

These results therefore highlight an important distinction between the statistical robustness and the computational efficiency of the method at different signal strengths. For signals below  $\text{SNR} 10$ , the method is unlikely to produce reliable results and we do not recommend its use. For signals with  $\text{SNR}$  between 10 and 20, the empirically calibrated widening factors are robust for most cases, and the final inference will be statistically consistent with the standard analysis, provided enough samples are drawn from `simple-pe` in the first step of our method to correctly capture small secondary features (as discussed in Section IV). However, as shown in Fig. 10, the performance in this regime is unreliable, with some analyses resulting in a slowdown. Therefore, for both statistical validity and computational efficiency,

we recommend the application of our method for the time being to signals with a network  $\text{SNR} > 20$ . While this represents a minority ( $\lesssim 10\%$ ) of current detections in GWTC-4.0, these high-SNR events are often the most information-rich signals and warrant repeated analyses to study carefully [110–112]. As such, they account for a disproportionate fraction of the total computational budget for parameter estimation. For future observing runs, and observatories like the Einstein Telescope, signals with  $\text{SNR} > 20$  are predicted to constitute a larger fraction of the observed population; for Einstein Telescope approximately 50% of all detections will have  $\text{SNR} > 20$  [113].

There is only one injection with  $\text{SNR} > 20$  that resulted in a per-sample slowdown, and it serves to illustrate the method’s robustness. This case, with  $\text{SNR} 23.5$ , is shown in Fig. 11. The slowdown occurred because the initial `simple-pe` approximation was offset from the true posterior, particularly in the inclination angle,  $\theta_{\text{JN}}$ . Figure 11 shows that the final posterior distributions from our method and the standard analysis are in excellent agreement. However, they lie partially in the tails of the widened repartitioned prior. Without this conservative widening, the initial approximation would have excluded regions of significant posterior probability, leading to a biased result. The additional computational cost arose from the inefficiency of having to sample this tail region of the flow to correctly converge to the posterior; although our method resulted in a lower KL divergence, the number of likelihood evaluations per nested sampling iteration was higher because of this. This event demonstrates a key strength of the method: by design, it sacrifices efficiency when necessary to guarantee statistically unbiased inference, which is possible due to the widening procedure developed in Section III C. This is also the reason that several injections between  $10 < \text{SNR} < 20$  are slower than the standard analysis. Again, this widening procedure is calibrated to be conservative and often over-widens the `simple-pe` distribution to ensure robustness. Automating the widening procedure in future, perhaps with the widening factor being a parameter that is sampled during the analysis in a manner similar to [43], would lead to better performance improvements.

A key advantage of `simple-pe` is that it is in general more robust to multi-modal posteriors, a common feature in gravitational-wave analysis that presents a significant challenge for other PR initialisation methods. A low-resolution NS run or a Fisher matrix approximation can both fail to identify secondary posterior modes, particularly when they are well-separated from the primary mode. Such a failure leads to biased inference, as the repartitioned prior can inadvertently exclude regions of significant posterior probability. Figure 12 provides a practical demonstration of our method’s strength in this scenario for an injection with a bimodal inclination angle. The `simple-pe` analysis successfully captures the bimodal structure of the posterior. This information is then passed to the repartitioned prior, which ensures the

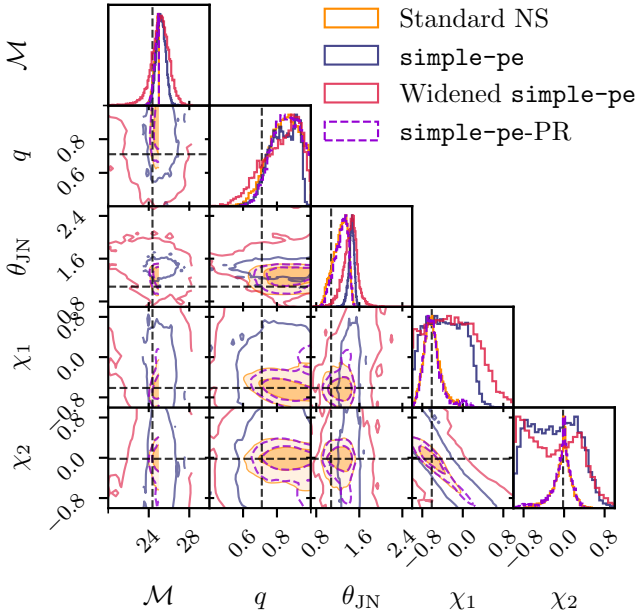


FIG. 11. A corner plot demonstrating the method’s robustness for the single high-SNR ( $\geq 20$ ) analysis that resulted in a slowdown. The initial **simple-pe** approximation is significantly offset from the marginal posterior in the inclination angle,  $\theta_{\text{JN}}$ , which was recovered by the standard NS analysis. The widened **simple-pe** distribution, used as the repartitioned prior, successfully contains this posterior. This ensures that the final **simple-pe-PR** posterior is in excellent agreement with the standard result. For visual clarity, the **simple-pe** and widened **simple-pe** distributions show only the  $3\sigma$  contours, while the final posteriors include the  $1\sigma$  and  $2\sigma$  contours.

subsequent NS analysis explores both modes and converges to the correct, unbiased posterior distribution. This case highlights how the physically-motivated model of **simple-pe** can provide a more reliable starting point for PR than a simple stochastic search, preserving the statistical integrity of the analysis for complex posterior geometries.

In summary, the injection study successfully validates our method. It produces statistically consistent posteriors across a broad parameter range, and its performance characteristics are consistent with the SNR scaling relationship established in Section IV.

## VI. CONCLUSIONS

The increasing detection rate and SNR of gravitational-wave events from the global detector network are enabling an era of high-precision science, but the computational cost of the required parameter estimation presents a significant challenge [11–13]. Standard nested sampling, while robust, is computationally expensive, particularly for the loudest signals.

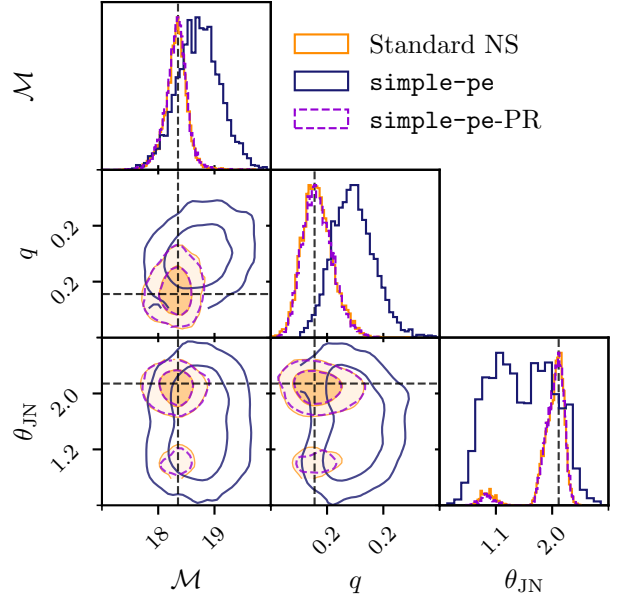


FIG. 12. A representative injection from the study with a bimodal marginal posterior for the inclination angle ( $\theta_{\text{JN}}$ ). The **simple-pe** approximation correctly identifies both modes of the posterior. This ensures the repartitioned prior encompasses the full posterior structure, including the secondary mode, leading to an unbiased final inference.

In this work, we have presented and validated a method to accelerate this process by combining the rapid, physically-motivated constraints from **simple-pe** with the nested sampling acceleration technique of posterior repartitioning.

An injection study, performed on a broad population drawn from standard analysis priors, rigorously validated the statistical integrity of our method. The successful probability-probability test and the detailed analysis of challenging cases confirm that our method produces unbiased posteriors consistent with standard techniques, correctly prioritising statistical robustness over speed when necessary.

We have established a clear relationship between SNR and performance, showing that the computational speedup increases with SNR. For a fiducial signal at an SNR of 150, we achieve a per-sample speedup factor of approximately 2.1 in the number of likelihood evaluations. By comparison, a signal produced by the same parameters but a smaller luminosity distance, with SNR 30, achieves a per-sample speedup of 1.2, showing that the efficiency grows significantly with signal strength. Furthermore, the per-sample speedup does not show signs of saturating at SNR 150, indicating that further gains are possible for yet louder signals. This positions our method as a powerful algorithm for next-generation signals from observatories like the Einstein Telescope and LISA [97–101].

Beyond the numerical speedup, our method provides

a way to capitalise on the standard GW analysis workflow. Low-latency analyses, like `simple-pe`, are essential for rapid event alerts, but the valuable information they provide about the likely region of parameter space is typically set aside when the final, high-fidelity parameter estimation is performed. This separation is necessary to preserve the integrity of the Bayesian prior, which must not be informed by the data being analysed. Our method provides an innovative strategy for this purpose. As a purely computational technique, it uses the low-latency result to focus the sampler on the region of interest, while the repartitioning factor (Eq. 3) mathematically ensures that the final posterior is identical to one produced from the original, unaltered prior. The method thus gains the efficiency of an informed analysis while rigorously preserving the statistical purity of the final inference.

The repartitioning algorithm presented here is not specific to `simple-pe`. It is possible to use our technique with machine learning algorithms, which also rapidly produce initial posterior estimates [26–31]. However, care should be taken when using initialisation methods which are not robust to multi-modal posteriors, such as a Fisher matrix approximation, as these could cut off secondary modes in the subsequent analysis and bias the inference. Our method is also complementary to likelihood acceleration techniques; `simple-pe-PR` reduces the number of required likelihood evaluations, and thus can be combined with optimised likelihoods that reduce the cost of each individual evaluation for even further speedups [47–50]. `simple-pe` could also be used to seed alternative sampling methods besides NS, such as Sequential Monte Carlo, to accelerate GW inference [72, 114]. An important future direction for this work is in automating the widening procedure, in order to improve both the robustness and the performance gains. Moreover, our method could be extended to explore precessing systems.

In summary, we have developed a robust algorithm for accelerating gravitational-wave parameter estimation in the high-SNR regime. This method focuses on speeding up the core nested sampling algorithm itself, meaning it can be used in conjunction with other established acceleration techniques for further gains. This work represents a substantial step towards preparing for the data analysis challenges of the next generation of gravitational-wave observatories and will help to realise the full scientific potential of future detections.

## ACKNOWLEDGMENTS

We thank Sama Al-Shammari for helpful comments during the LIGO–Virgo–KAGRA internal review. We additionally thank Stephen Fairhurst, Laura Nuttall and Mukesh Singh for valuable discussions, and Stephen Fairhurst and Mukesh Singh for their continued development of `simple-pe` (alongside C.H). M.P was supported by the research environment and infrastructure of the Handley Lab at the University of Cambridge. C.H

thanks the UKRI Future Leaders Fellowship for support through the grant MR/T01881X/1, and the University of Portsmouth for support through the Dennis Sciama Fellowship. M.J.W acknowledges support from ST/X002225/1, ST/Y004876/1 and the University of Portsmouth. For the purpose of open access, the author(s) has applied a Creative Commons Attribution (CC BY) licence to any Author Accepted Manuscript version arising.

This work was performed using the Cambridge Service for Data Driven Discovery (CSD3), part of which is operated by the University of Cambridge Research Computing on behalf of the STFC DiRAC HPC Facility ([www.dirac.ac.uk](http://www.dirac.ac.uk)). The DiRAC component of CSD3 was funded by BEIS capital funding via STFC capital grants ST/P002307/1 and ST/R002452/1 and STFC operations grant ST/R00689X/1. DiRAC is part of the National e-Infrastructure.

This work made use of `numpy` [115], `scipy` [82], `simple-pe` [42], `pesummary` [116], `bilby=2.3.0` [56, 117], `anesthetic` [118] and `margarine` [79, 80]. Plots were prepared with `matplotlib` [119] and `anesthetic` [118].

Parameter	Shape	Range
Chirp mass ( $\mathcal{M}_c$ )	Uniform (comp)	$[10, 25] M_{\odot}$
Mass ratio ( $q$ )	Uniform (comp)	$[0.05, 1.0]$
Luminosity distance ( $d_L$ )	Uniform (source)	$[100, 1000] \text{ Mpc}$
Right ascension ( $\alpha$ )	Uniform	$[0, 2\pi] \text{ rad}$
Declination ( $\delta$ )	Cosine	$[-\pi/2, \pi/2] \text{ rad}$
Inclination angle ( $\theta_{\text{JN}}$ )	Sine	$[0, \pi] \text{ rad}$
Polarization angle ( $\psi$ )	Uniform	$[0, \pi] \text{ rad}$
Phase at coalescence ( $\phi$ )	Uniform	$[0, 2\pi] \text{ rad}$
Spin of lighter BH ( $\chi_1$ )	Uniform (aligned)	$[-0.99, 0.99]$
Spin of heavier BH ( $\chi_2$ )	Uniform (aligned)	$[-0.99, 0.99]$
Time of coalescence ( $t_c$ )	Uniform	trigger time + $[-0.1, +0.1] \text{ s}$

TABLE III. Prior distributions for the 100 injections used in the injection study. The choice of a source-frame uniform luminosity distance prior and uniform component (comp) mass priors are chosen to be consistent with standard LVK analyses.

### Appendix A: Priors

The prior distributions used for the main nested sampling analyses, detailed in Table III, are chosen to be consistent with standard LVK priors for 8 second signals [120]. This includes priors that are uniform in the component masses, though the sampler itself explores the parameter space in terms of chirp mass and mass ratio. In contrast, the `simple-pe` analysis that initialises our method uses priors uniform in chirp mass and mass ratio directly. Similarly, the sampling priors on the spins are distributed uniformly over the sphere, whereas `simple-pe` uses a uniform prior on the effective aligned spin of the binary.

While this mismatch does not affect the statistical validity of the final posterior, our investigations show that it may have an impact on the computational efficiency of the method. The initial posterior approximation from `simple-pe` is conditioned on its own prior. Therefore, when the final analysis uses a different prior, the `simple-pe` guess can be more offset from the target posterior. This may necessitate more significant widening of the repartitioned prior and results in a larger effective KL divergence for the sampler to traverse, reducing the overall speedup.

Improved performance could be achieved in future work by using consistent priors throughout the method. This could be accomplished by adapting `simple-pe` to use component-mass priors or by implementing a prior re-weighting scheme for the initial samples before they are used to train the normalizing flow.

### Appendix B: Empirical Calibration of the Widening Factors

To ensure the repartitioned prior robustly encompasses the true posterior, the initial distribution from

`simple-pe` must be widened. We detail here the empirical procedure used to calibrate the widening factors applied throughout this work.

The calibration was performed using the 100-injection set described in Section V. For each injection, we determined the minimum widening required for the repartitioned prior to be statistically consistent with the posterior from the standard NS analysis. The procedure was as follows. First, a normalizing flow was trained on the initial `simple-pe` samples. Then, the standard deviation of each diagonal element of the flow's base covariance matrix was systematically increased. This process was repeated until the 1st and 99th percentiles of the standard NS posterior were contained within the 1st and 99th percentiles of the distribution generated by the widened flow. This calibration was performed independently for each repartitioned parameter.

The minimum required widening factor for each parameter is shown as a function of network SNR in Fig. 13. The results show a clear dependence on SNR for several parameters, particularly the chirp mass and spins, with a notable change in behavior around an SNR of 20. For many signals, especially those above SNR 10, little to no widening was required. Based on these results, we adopted the two sets of fixed, conservative widening factors detailed in Table II.

These widening factors were chosen to be robust against the small, expected variations between the `simple-pe` approximation and the true posterior. We note that these factors are not tuned to accommodate rare outlier cases where the initial guess is significantly offset (as in the examples discussed in Section V). A more advanced implementation could employ an automated widening procedure, where the widening factors themselves are sampled during the analysis. This would be robust to outliers, applying large widening only when needed, while retaining higher efficiency for typical cases where minimal widening is sufficient. We leave the development of such a widening procedure for future work.

### Appendix C: KL Divergences and PR Speedups

The performance scaling of our method, presented in Section IV, can be understood better through considering the Kullback-Leibler (KL) divergence. In the context of nested sampling, the KL divergence between the sampling prior and the posterior,  $D_{\text{KL}}(\mathcal{P} \parallel \pi)$ , quantifies the information gain, or the ‘amount of compression’, required for the sampler to converge from the prior to the posterior [38, 43, 68]. A larger KL divergence generally corresponds to a longer and more computationally expensive nested sampling run. By design, our method aims to reduce this divergence by replacing the broad original prior with a more compact repartitioned prior that is already a closer approximation of the posterior.

Figure 14 plots the change in the KL divergence between our method and the standard NS analysis for the

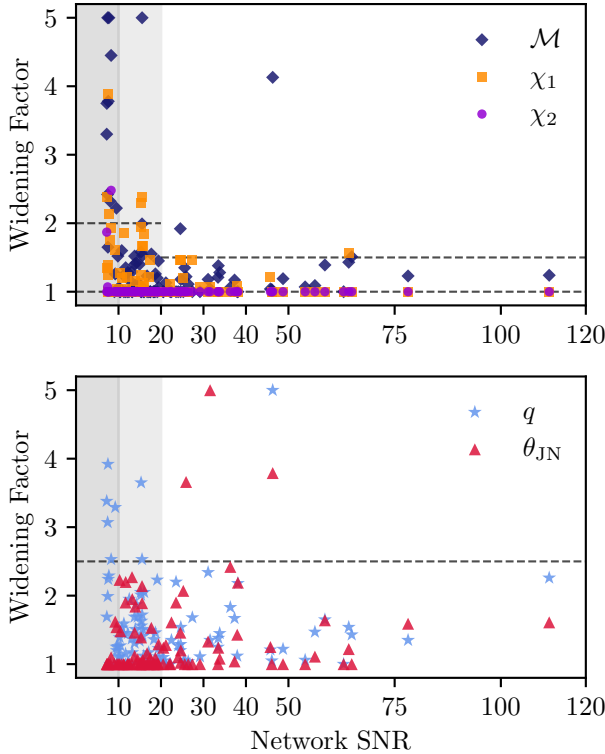


FIG. 13. The minimum widening factor required for the repartitioned prior to encompass the 1st and 99th percentiles of the standard nested sampling posterior for each of the 100 injections. The widening factor represents the multiplicative value applied to the standard deviation of the normalizing flow’s base distribution for a given parameter. These results were used to calibrate the two sets of fixed, conservative factors used in this work (dashed lines).

SNR scaling study. The results provide further insight into the observed performance. At SNR 10, the substantial widening applied to the already broad `simple-pe` guess results in a repartitioned prior that is a poorer representation of the posterior than the original prior. This causes the KL divergence to increase, leading to the performance reduction reported in Section IV. For  $\text{SNR} \geq 20$ , our method successfully reduces the KL divergence. However, at SNR 20 specifically, this gain is offset by the sampling inefficiency introduced by the missed secondary posterior mode, which explains the slight performance reduction in this case. For  $\text{SNR} \geq 30$ , the performance gains are driven directly by the reduction in KL divergence. The growing difference in KL divergence between our method and the standard analysis as SNR increases is the underlying reason for the trend of increasing speedups.

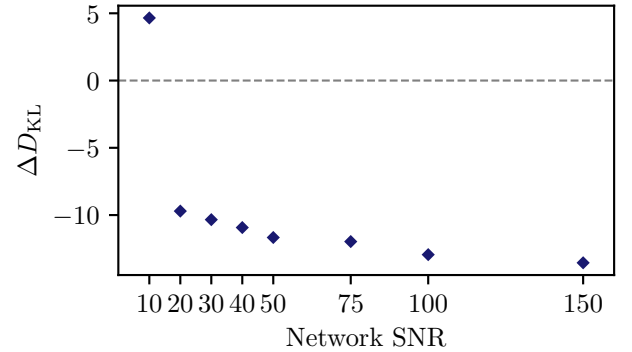


FIG. 14. The change in the KL divergence between the sampling prior and posterior for our method relative to the standard NS analysis. A negative value indicates a reduction in the KL divergence for our method and an expected speedup. The plot shows that the method increases the required ‘compression’ at SNR 10 but successfully reduces it for all higher SNRs, providing an explanation for the performance trend observed in Section IV.

#### Appendix D: Jensen-Shannon Divergences

To quantitatively assess the statistical consistency between the posteriors from standard NS and our `simple-pe-PR` method, we compute the Jensen-Shannon Divergence (JSD) for the one-dimensional marginal distributions.

To estimate the mean and uncertainty of the JSD for each comparison, we generate 100 posterior realisations per analysis. This is achieved by resampling the nested sampling weights associated with the full set of dead points, using the functionality in `anesthetic` [118]. From each set of newly weighted points, a final realisation of 5000 posterior samples is produced via rejection sampling. The JSD is then calculated between kernel density estimates of these marginal distributions, constructed using `PESummary` [121]. JSD values below 0.05 bits, or 35 millinats, indicate that the distributions are statistically consistent [122].

The JSD values for the SNR scaling study are presented in Table IV. For all signals with  $\text{SNR} > 10$ , the JSDs are below this threshold, confirming excellent agreement between the methods. As expected from the discussion in Section IV, the SNR 10 signal exhibits a JSD value above the threshold, for the mass ratio parameter, providing a quantitative measure of the observed disagreement.

The JSD values for the full injection study are presented in Fig. 15. The results show a clear trend with SNR and provide quantitative support for the conclusions drawn in the main text. Below SNR 10, several injections exhibit JSDs above the 35 millinat threshold for consistency. This is expected, as our empirical widening factors were not calibrated for this low-SNR regime and can be insufficient to fully encompass the true posterior. In the

$10 \leq \text{SNR} < 20$  regime, the agreement improves significantly, though a few analyses still produce posteriors that are statistically distinguishable from the standard result. For signals with  $\text{SNR} > 20$ , only two injections fail the JSD test. These correspond to the specific outlier cases identified in Section V, where a significant offset in the initial `simple-pe` guess was not fully corrected by the widening procedure. An automated widening scheme would likely resolve these remaining discrepancies. These results provide quantitative evidence for our recommendation to apply the method to signals with  $\text{SNR} > 20$ , the regime where it is both computationally efficient and statistically robust.

## Appendix E: Effective Sample Size

The effective sample size from a nested sampling analysis can be obtained using the set of nested sampling weights,  $w_i$ , for each dead point,  $i$ . This can be calculated as [102]:

$$n_{\text{eff}} = \frac{(\sum_i w_i)^2}{\sum_i w_i^2}. \quad (\text{E1})$$

Posterior repartitioned NS typically spends a longer time exploring the bulk of the posterior than standard NS for a given number of live points (see Figure 16). This can be explained by PR having a greater density of points in this region, due to the smaller effective prior volume. Thus, the rate of prior volume compression occurs more slowly in this region, generating a larger number of dead points with non-negligible weights, and therefore resulting in a larger effective sample size. As a result, our method should be performed with fewer live points than a standard NS analysis in order to obtain a given final sample size.

## Appendix F: P-P Plot for Standard NS with `dynesty`

The P-P plot obtained from standard NS on our injection set from Section V is shown in Figure 17. The p-values for each parameter are similar to those from our method and, as mentioned in Section V, the p-values between the two sets of P-P distributions for each parameter are all above 0.9, indicating excellent agreement on a population level between the two methods.

---

[1] A. G. Abac *et al.* (LIGO Scientific, VIRGO, KAGRA), GWTC-4.0: Methods for Identifying and Characterizing Gravitational-wave Transients, arXiv:2508.18081 (2025), arXiv:2508.18081 [gr-qc].

[2] A. G. Abac *et al.* (LIGO Scientific, VIRGO, KAGRA), GWTC-4.0: Population Properties of Merging Compact Binaries, arXiv:2508.18083 (2025), arXiv:2508.18083 [astro-ph.HE].

[3] A. G. Abac *et al.* (LIGO Scientific, VIRGO, KAGRA), GWTC-4.0: Constraints on the Cosmic Expansion Rate and Modified Gravitational-wave Propagation, arXiv:2509.04348 (2025), arXiv:2509.04348 [astro-ph.CO].

[4] R. Abbott *et al.* (LIGO Scientific, VIRGO, KAGRA), Tests of General Relativity with GWTC-3, Phys. Rev. D **112**, 084080 (2025), arXiv:2112.06861 [gr-qc].

[5] A. Ray and V. Kalogera, Reexamining Evidence of a Pair-Instability Mass Gap in the Binary Black Hole Population, arXiv:2510.18867 (2025), arXiv:2510.18867 [astro-ph.HE].

[6] A. Hussain, M. Isi, and A. Zimmerman, Living on the edge: Testing for compact population features at the edges of parameter space, arXiv:2510.20010 (2025), arXiv:2510.20010 [astro-ph.IM].

[7] H. Tong, T. A. Callister, M. Fishbach, E. Thrane, F. Antonini, S. Stevenson, I. M. Romero-Shaw, and F. Dosopoulou, A subpopulation of low-mass, spinning black holes: signatures of dynamical assembly, arXiv:2511.05316 (2025), arXiv:2511.05316 [astro-ph.HE].

[8] N. V. Krishnendu, F. Ohme, and K. G. Arun, Testing the nature of compact objects in the lower mass gap using gravitational wave observations, arXiv:2509.10420 (2025), arXiv:2509.10420 [astro-ph.HE].

[9] C. Adamcewicz, N. Guttman, P. D. Lasky, and E. Thrane, Do both black holes spin in merging binaries? Evidence from GWTC-4 and astrophysical implications, arXiv:2509.04706 (2025), arXiv:2509.04706 [astro-ph.HE].

[10] J. Stegmann and J. Klencki, Orbital Eccentricity and Spin–Orbit Misalignment Are Evidence that Neutron Star–Black Hole Mergers Form through Triple Star Evolution, Astrophys. J. Lett. **991**, L54 (2025), arXiv:2506.09121 [astro-ph.HE].

[11] The LIGO Scientific Collaboration *et al.*, Advanced ligo, Classical and Quantum Gravity **32**, 074001 (2015).

[12] F. Acernese, M. Agathos, K. Agatsuma, D. Aisa, N. Allemandou, A. Allocca, J. Amarni, P. Astone, G. Balestri, G. Ballardin, *et al.*, Advanced virgo: a second-generation interferometric gravitational wave detector, Classical and Quantum Gravity **32**, 024001 (2014).

[13] B. P. Abbott *et al.* (KAGRA, LIGO Scientific, Virgo, VIRGO), Prospects for observing and localizing gravitational-wave transients with Advanced LIGO, Advanced Virgo and KAGRA, Living Rev. Rel. **23**, 3 (2020), arXiv:1304.0670 [gr-qc].

[14] J. Aasi *et al.* (LIGO Scientific), Advanced LIGO, Class. Quant. Grav. **32**, 074001 (2015), arXiv:1411.4547 [gr-qc].

[15] F. Acernese *et al.* (VIRGO), Advanced Virgo: a second-generation interferometric gravitational wave detector, Class. Quant. Grav. **32**, 024001 (2015), arXiv:1408.3978 [gr-qc].

[16] T. Akutsu *et al.* (KAGRA), Overview of KAGRA: Detector design and construction history, PTEP **2021**,

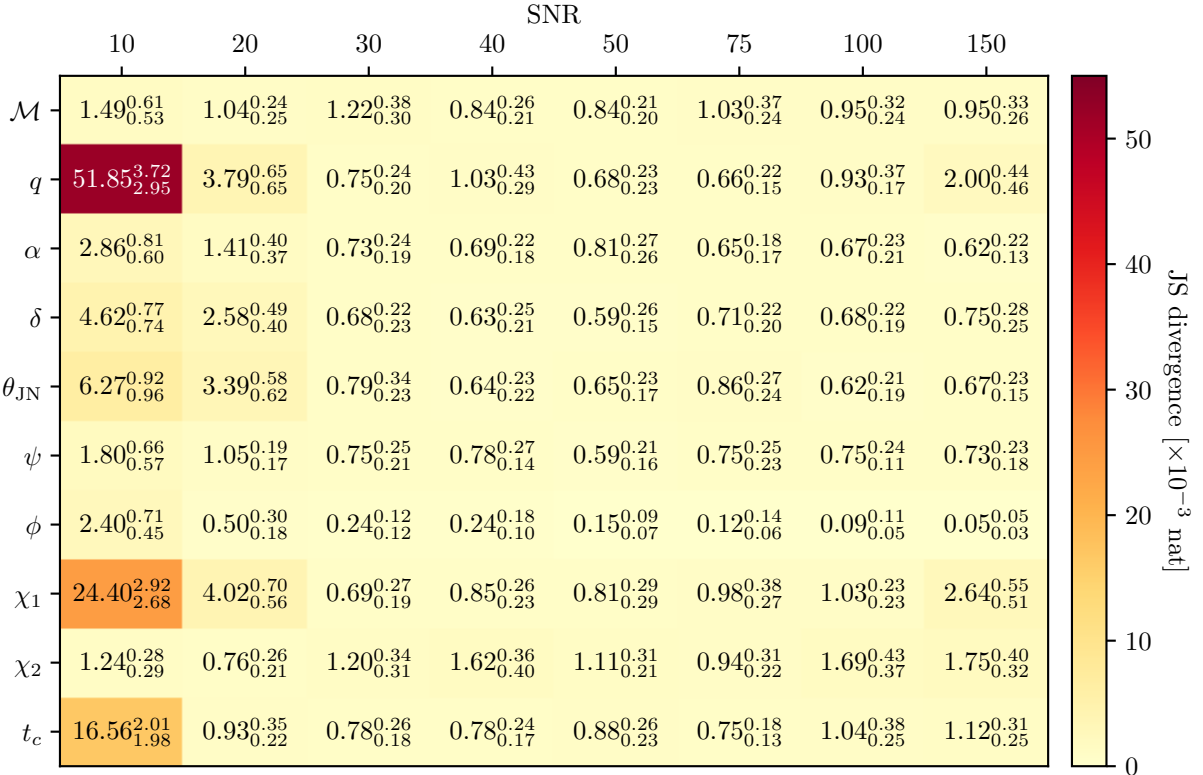


TABLE IV. Jensen-Shannon divergences for marginal posterior distributions between standard NS and our method, from the SNR scaling study. The quoted values are in units of  $1 \times 10^{-3}$  nats. 100 different realisations of 5000 posterior samples were generated for each analysis by resampling the nested sampling weights and performing rejecting sampling again. The mean and  $1\sigma$  quantiles are shown, where for injections above SNR 10 the JSD values are within the threshold of 0.05 bits, or 35 millinats [122]. There are significant disagreements for the SNR 10 signal for the mass ratio parameter, but we do not recommend the application of our method in this SNR regime.

05A101 (2021), arXiv:2005.05574 [physics.ins-det].

- [17] B. Iyer *et al.*, Ligo-india, proposal of the consortium for indian initiative in gravitational-wave observations (indigo), DCC (2011).
- [18] J. Lange, R. O’Shaughnessy, and M. Rizzo, Rapid and accurate parameter inference for coalescing, precessing compact binaries, arXiv:1805.10457 (2018), arXiv:1805.10457 [gr-qc].
- [19] J. Roulet, J. Mushkin, D. Wadekar, T. Venumadhav, B. Zackay, and M. Zaldarriaga, Fast marginalization algorithm for optimizing gravitational wave detection, parameter estimation, and sky localization, Phys. Rev. D **110**, 044010 (2024), arXiv:2404.02435 [gr-qc].
- [20] C. Pankow, P. Brady, E. Ochsner, and R. O’Shaughnessy, Novel scheme for rapid parallel parameter estimation of gravitational waves from compact binary coalescences, Phys. Rev. D **92**, 023002 (2015), arXiv:1502.04370 [gr-qc].
- [21] L. Pathak, A. Reza, and A. S. Sengupta, Fast likelihood evaluation using meshfree approximations for reconstructing compact binary sources, Phys. Rev. D **108**, 064055 (2023), arXiv:2210.02706 [gr-qc].
- [22] V. Tiwari, C. Hoy, S. Fairhurst, and D. MacLeod, Fast non-Markovian sampler for estimating gravitational-wave posteriors, Phys. Rev. D **108**, 023001 (2023), arXiv:2303.01463 [astro-ph.HE].
- [23] A. H. Nitz, Robust, rapid, and simple gravitational-wave parameter estimation, Phys. Rev. D **112**, 023032 (2025), arXiv:2410.05190 [astro-ph.IM].
- [24] A. Sharma, L. Pathak, S. Roy, and A. S. Sengupta, Rapid parameter estimation with the full symphony of compact binary mergers using meshfree approximation, arXiv:2508.04172 (2025), arXiv:2508.04172 [gr-qc].
- [25] J. Mushkin, J. Roulet, B. Zackay, T. Venumadhav, O. Ivashtenko, D. Wadekar, A. K. Mehta, and M. Zaldarriaga, Sampler-free gravitational wave inference using matrix multiplication, Phys. Rev. D **112**, 104025 (2025), arXiv:2507.16022 [gr-qc].
- [26] H. Gabbard, C. Messenger, I. S. Heng, F. Tonolini, and R. Murray-Smith, Bayesian parameter estimation using conditional variational autoencoders for gravitational-wave astronomy, Nature Phys. **18**, 112 (2022), arXiv:1909.06296 [astro-ph.IM].
- [27] S. R. Green and J. Gair, Complete parameter inference for GW150914 using deep learning, Mach. Learn. Sci. Tech. **2**, 03LT01 (2021), arXiv:2008.03312 [astro-ph.IM].
- [28] S. R. Green, C. Simpson, and J. Gair, Gravitational-wave parameter estimation with autoregressive neural network flows, Phys. Rev. D **102**, 104057 (2020), arXiv:2006.08830 [astro-ph.IM].

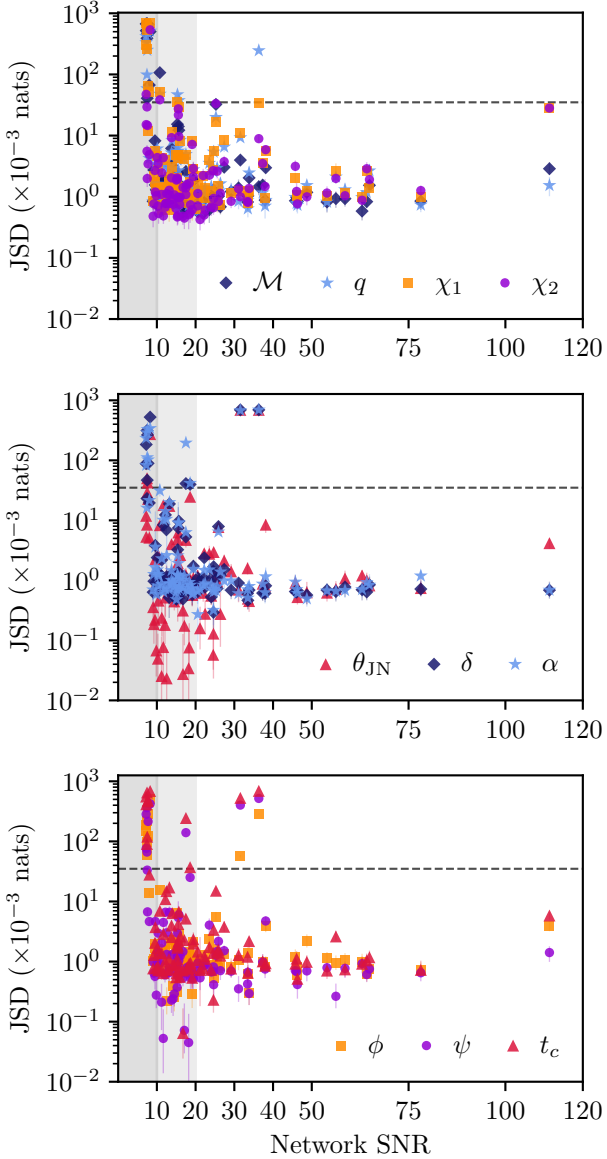


FIG. 15. The Jensen-Shannon divergence (JSD) between the one-dimensional marginal posteriors from our method and the standard NS analysis for each of the 100 injections. Each point represents the JSD for a single parameter and for a single event. The horizontal dashed line at 35 millinats represents the threshold for statistical consistency [122]. The plot shows a clear trend of improved agreement at higher SNR.

arXiv:2002.07656 [astro-ph.IM].

[29] M. Dax, S. R. Green, J. Gair, J. H. Macke, A. Buonanno, and B. Schölkopf, Real-Time Gravitational Wave Science with Neural Posterior Estimation, *Phys. Rev. Lett.* **127**, 241103 (2021), arXiv:2106.12594 [gr-qc].

[30] M. Dax, S. R. Green, J. Gair, N. Gupte, M. Pürer, V. Raymond, J. Wildberger, J. H. Macke, A. Buonanno, and B. Schölkopf, Real-time inference for binary neutron star mergers using machine learning, *Nature* **639**, 49 (2025), arXiv:2407.09602 [gr-qc].

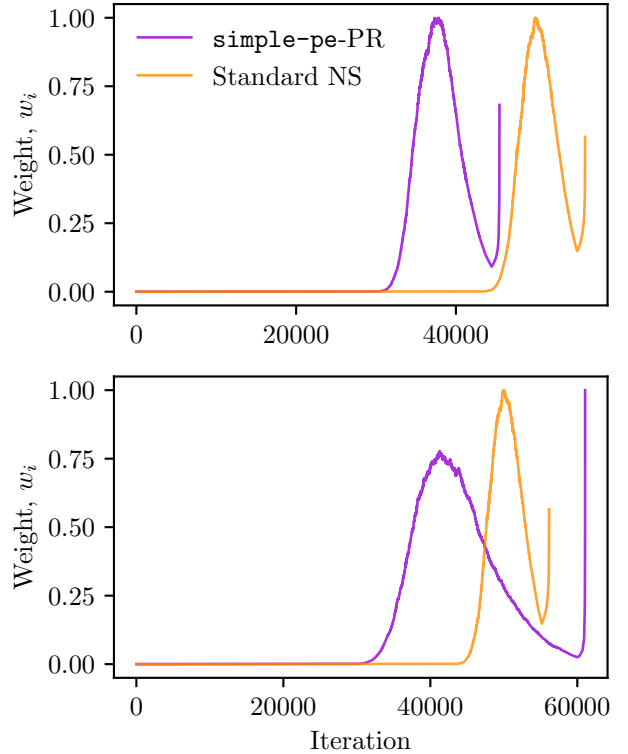


FIG. 16. Comparison of the posterior weight distribution of the dead points for a standard NS analysis (orange) and our **simple-pe-PR** method (violet). The x-axis represents the nested sampling iteration, and the y-axis is the posterior weight. The top panel shows a typical case where the PR analysis enters the high-likelihood region (where weights become non-negligible) earlier but the phase of significant weight extends over slightly more iterations, resulting in a larger effective sample size. The bottom panel shows a more extreme case where the compression through the posterior is much slower for the PR analysis, leading to a substantially larger effective sample size at the cost of a longer runtime. Both cases demonstrate that a direct comparison of runtimes at a fixed number of live points is misleading, and the per-sample speedup is a more informative metric.

[31] V. Raymond, S. Al-Shammari, and A. Göttel, Simulation-based Inference for Gravitational-waves from Intermediate-Mass Binary Black Holes in Real Noise, *Mon. Not. Roy. Astron. Soc.* **1103**, 1108 (2025), arXiv:2406.03935 [gr-qc].

[32] A. G. Abac *et al.* (LIGO Scientific, Virgo, KAGRA), GW250114: Testing Hawking’s Area Law and the Kerr Nature of Black Holes, *Phys. Rev. Lett.* **135**, 111403 (2025), arXiv:2509.08054 [gr-qc].

[33] Black Hole Spectroscopy and Tests of General Relativity with GW250114, arXiv:2509.08099 (2025), arXiv:2509.08099 [gr-qc].

[34] E. Thrane and C. Talbot, An introduction to bayesian inference in gravitational-wave astronomy: Parameter estimation, model selection, and hierarchical models, *Publications of the Astronomical Society of Australia* **36**, 10.1017/pasa.2019.2 (2019).

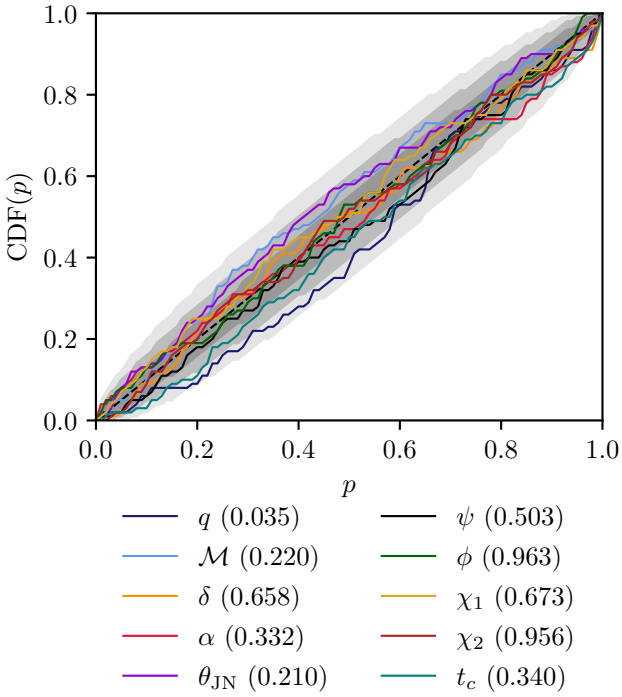


FIG. 17. P-P plot obtained from the standard nested sampling analyses performed on our injection set from Section V using the `dynesty` sampler.

- [35] J. Veitch, V. Raymond, B. Farr, W. Farr, P. Graff, S. Vitale, B. Aylott, K. Blackburn, N. Christensen, M. Coughlin, W. Del Pozzo, F. Feroz, J. Gair, C.-J. Haster, V. Kalogera, T. Littenberg, I. Mandel, R. O’Shaughnessy, M. Pitkin, C. Rodriguez, C. Röver, T. Sidery, R. Smith, M. Van Der Sluys, A. Vecchio, W. Vausden, and L. Wade, Parameter estimation for compact binaries with ground-based gravitational-wave observations using the `lalinference` software library, *Physical Review D* **91**, 10.1103/physrevd.91.042003 (2015).
- [36] J. Skilling, Nested Sampling, *AIP Conf. Proc.* **735**, 395 (2004).
- [37] J. Skilling, Nested sampling for general Bayesian computation, *Bayesian Analysis* **1**, 833 (2006).
- [38] J. Skilling, Nested sampling for general Bayesian computation, *Bayesian Analysis* **1**, 833 (2006).
- [39] B. P. Abbott *et al.*, A guide to ligo-virgo detector noise and extraction of transient gravitational-wave signals, *Classical and Quantum Gravity* **37**, 055002 (2020).
- [40] X. Chen, M. Hobson, S. Das, and P. Gelderblom, Improving the efficiency and robustness of nested sampling using posterior repartitioning (2018), arXiv:1803.06387 [stat.CO].
- [41] X. Chen, F. Feroz, and M. Hobson, Bayesian posterior repartitioning for nested sampling (2022), arXiv:1908.04655 [stat.CO].
- [42] S. Fairhurst, C. Hoy, R. Green, C. Mills, and S. A. Usman, Simple parameter estimation using observable features of gravitational-wave signals (2023), arXiv:2304.03731 [gr-qc].

- [43] M. Prathaban, H. Bevins, and W. Handley, Accelerated nested sampling with posterior repartitioning and  $\beta$ -flows for gravitational waves, *Monthly Notices of the Royal Astronomical Society*, staf962 (2025), <https://academic.oup.com/mnras/advance-article-pdf/doi/10.1093/mnras/staf962/63500183/staf962.pdf>.
- [44] T. A. Apostolatos, C. Cutler, G. J. Sussman, and K. S. Thorne, Spin induced orbital precession and its modulation of the gravitational wave forms from merging binaries, *Phys. Rev. D* **49**, 6274 (1994).
- [45] J. N. Goldberg, A. J. MacFarlane, E. T. Newman, F. Rohrlich, and E. C. G. Sudarshan, Spin- $s$  spherical harmonics and  $\delta$ , *J. Math. Phys.* **8**, 2155 (1967).
- [46] K. S. Thorne, Multipole Expansions of Gravitational Radiation, *Rev. Mod. Phys.* **52**, 299 (1980).
- [47] N. J. Cornish, Heterodyned likelihood for rapid gravitational wave parameter inference, *Phys. Rev. D* **104**, 104054 (2021), arXiv:2109.02728 [gr-qc].
- [48] P. Canizares, S. E. Field, J. Gair, V. Raymond, R. Smith, and M. Tiglio, Accelerated gravitational-wave parameter estimation with reduced order modeling, *Phys. Rev. Lett.* **114**, 071104 (2015), arXiv:1404.6284 [gr-qc].
- [49] S. Vinciguerra, J. Veitch, and I. Mandel, Accelerating gravitational wave parameter estimation with multi-band template interpolation, *Classical and Quantum Gravity* **34**, 115006 (2017).
- [50] S. Morisaki, Accelerating parameter estimation of gravitational waves from compact binary coalescence using adaptive frequency resolutions, *Physical Review D* **104**, 10.1103/physrevd.104.044062 (2021).
- [51] G. Ashton and T. Dietrich, The use of hypermodels to understand binary neutron star collisions, *Nature Astron.* **6**, 961 (2022), arXiv:2111.09214 [gr-qc].
- [52] C. Hoy, Accelerating multimodel Bayesian inference, model selection, and systematic studies for gravitational wave astronomy, *Phys. Rev. D* **106**, 083003 (2022), arXiv:2208.00106 [gr-qc].
- [53] C. Hoy, S. Akcay, J. Mac Uilliam, and J. E. Thompson, Incorporation of model accuracy in gravitational wave Bayesian inference, *Nature Astron.* **9**, 1256 (2025), arXiv:2409.19404 [gr-qc].
- [54] W. K. Hastings, Monte carlo sampling methods using Markov chains and their applications, *Biometrika* **57**, 97 (1970).
- [55] G. Ashton and C. Talbot, `jscipybilbyjscipy-mcmc`: an mcmc sampler for gravitational-wave inference, *Monthly Notices of the Royal Astronomical Society* **507**, 2037–2051 (2021).
- [56] G. Ashton *et al.*, BILBY: A user-friendly Bayesian inference library for gravitational-wave astronomy, *Astrophys. J. Suppl.* **241**, 27 (2019), arXiv:1811.02042 [astro-ph.IM].
- [57] J. S. Speagle, `dynesty`: a dynamic nested sampling package for estimating bayesian posteriors and evidences, *Monthly Notices of the Royal Astronomical Society* **493**, 3132–3158 (2020).
- [58] M. J. Williams, J. Veitch, and C. Messenger, Nested sampling with normalizing flows for gravitational-wave inference, *Phys. Rev. D* **103**, 103006 (2021), arXiv:2102.11056 [gr-qc].
- [59] R. J. E. Smith, G. Ashton, A. Vajpeyi, and C. Talbot, Massively parallel Bayesian inference for transient gravitational-wave astronomy, *Mon. Not. Roy. Astron.*

Soc. **498**, 4492 (2020), arXiv:1909.11873 [gr-qc].

[60] N. J. Cornish, Fast Fisher Matrices and Lazy Likelihoods, arXiv:1007.4820 (2010), arXiv:1007.4820 [gr-qc].

[61] R. Smith, S. E. Field, K. Blackburn, C.-J. Haster, M. Pürer, V. Raymond, and P. Schmidt, Fast and accurate inference on gravitational waves from precessing compact binaries, Phys. Rev. D **94**, 044031 (2016), arXiv:1604.08253 [gr-qc].

[62] S. Vinciguerra, J. Veitch, and I. Mandel, Accelerating gravitational wave parameter estimation with multi-band template interpolation, Class. Quant. Grav. **34**, 115006 (2017), arXiv:1703.02062 [gr-qc].

[63] B. Zackay, L. Dai, and T. Venumadhav, Relative Binning and Fast Likelihood Evaluation for Gravitational Wave Parameter Estimation, arXiv:1806.08792 (2018), arXiv:1806.08792 [astro-ph.IM].

[64] S. Morisaki, Accelerating parameter estimation of gravitational waves from compact binary coalescence using adaptive frequency resolutions, Phys. Rev. D **104**, 044062 (2021), arXiv:2104.07813 [gr-qc].

[65] S. Morisaki, R. Smith, L. Tsukada, S. Sachdev, S. Stevenson, C. Talbot, and A. Zimmerman, Rapid localization and inference on compact binary coalescences with the Advanced LIGO-Virgo-KAGRA gravitational-wave detector network, Phys. Rev. D **108**, 123040 (2023), arXiv:2307.13380 [gr-qc].

[66] Q. Hu and J. Veitch, Costs of bayesian parameter estimation in third-generation gravitational wave detectors: a review of acceleration methods (2024), arXiv:2412.02651 [gr-qc].

[67] C. Hoy and L. K. Nuttall, BILBY in space: Bayesian inference for transient gravitational-wave signals observed with LISA, Mon. Not. Roy. Astron. Soc. **529**, 3052 (2024), arXiv:2312.13039 [astro-ph.IM].

[68] A. Petrosyan and W. Handley, Supernest: accelerated nested sampling applied to astrophysics and cosmology (2022).

[69] G. Papamakarios, E. Nalisnick, D. J. Rezende, S. Mohamed, and B. Lakshminarayanan, Normalizing flows for probabilistic modeling and inference (2021), arXiv:1912.02762 [stat.ML].

[70] I. Kobyzhev, S. J. Prince, and M. A. Brubaker, Normalizing flows: An introduction and review of current methods, IEEE Transactions on Pattern Analysis and Machine Intelligence **43**, 3964–3979 (2021).

[71] N. E. Wolfe, C. Talbot, and J. Golomb, Accelerating tests of general relativity with gravitational-wave signals using hybrid sampling, Phys. Rev. D **107**, 104056 (2023), arXiv:2208.12872 [gr-qc].

[72] M. J. Williams, Accelerated sequential posterior inference via reuse for gravitational-wave analyses (2025), arXiv:2511.04218 [hep-ex].

[73] C. Hoy, C. R. Weaving, L. K. Nuttall, and I. Harry, A rapid multi-modal parameter estimation technique for LISA, Class. Quant. Grav. **41**, 245012 (2024), arXiv:2408.12764 [gr-qc].

[74] B. G. Patterson, S. M. Tomson, and S. Fairhurst, Identifying eccentricity in binary black hole mergers using a harmonic decomposition of the gravitational waveform, Phys. Rev. D **111**, 044073 (2025), arXiv:2411.04187 [gr-qc].

[75] B. J. Owen, Search templates for gravitational waves from inspiraling binaries: Choice of template spacing, Phys. Rev. D **53**, 6749 (1996), arXiv:gr-qc/9511032.

[76] S. Fairhurst, R. Green, C. Hoy, M. Hannam, and A. Muir, Two-harmonic approximation for gravitational waveforms from precessing binaries, Phys. Rev. D **102**, 024055 (2020), arXiv:1908.05707 [gr-qc].

[77] C. McIsaac, C. Hoy, and I. Harry, Search technique to observe precessing compact binary mergers in the advanced detector era, Phys. Rev. D **108**, 123016 (2023), arXiv:2303.17364 [gr-qc].

[78] R. Ursell, C. Hoy, I. Harry, and L. K. Nuttall, The Missing Multipole Problem: Investigating biases from model starting frequency in gravitational-wave analyses, arXiv:2510.15048 (2025), arXiv:2510.15048 [gr-qc].

[79] H. Bevins, W. Handley, P. Lemos, P. Sims, E. de Lera Acedo, and A. Fialkov, Marginal Bayesian Statistics Using Masked Autoregressive Flows and Kernel Density Estimators with Examples in Cosmology, arXiv e-prints , arXiv:2207.11457 (2022), arXiv:2207.11457 [astro-ph.CO].

[80] H. T. J. Bevins, W. J. Handley, P. Lemos, P. H. Sims, E. de Lera Acedo, A. Fialkov, and J. Alsing, Marginal post-processing of Bayesian inference products with normalizing flows and kernel density estimators, **526**, 4613 (2023), arXiv:2205.12841 [astro-ph.IM].

[81] M. Prathaban and H. Bevins, margarine\_unbounded: A fork of margarine with support for unbounded distributions, [https://github.com/mrosep/margarine\\_unbounded](https://github.com/mrosep/margarine_unbounded) (2026).

[82] P. Virtanen, R. Gommers, T. E. Oliphant, M. Haberland, T. Reddy, D. Cournapeau, E. Burovski, P. Peterson, W. Weckesser, J. Bright, S. J. van der Walt, M. Brett, J. Wilson, K. J. Millman, N. Mayorov, A. R. J. Nelson, E. Jones, R. Kern, E. Larson, C. J. Carey, I. Polat, Y. Feng, E. W. Moore, J. VanderPlas, D. Laxalde, J. Perktold, R. Cimrman, I. Henriksen, E. A. Quintero, C. R. Harris, A. M. Archibald, A. H. Ribeiro, F. Pedregosa, P. van Mulbregt, and SciPy 1.0 Contributors, SciPy 1.0: Fundamental Algorithms for Scientific Computing in Python, Nature Methods **17**, 261 (2020).

[83] V. D’Emilio, R. Green, and V. Raymond, Density estimation with Gaussian processes for gravitational wave posteriors, Mon. Not. Roy. Astron. Soc. **508**, 2090 (2021), arXiv:2104.05357 [gr-qc].

[84] We note that `simple-pe` is still in active development and it is possible that in the future this widening procedure will not be required to obtain robust results.

[85] M. Prathaban, C. Hoy, and M. J. Williams, `bilby-pr`: v0.1.0 (2026).

[86] Although we note that `simple-pe` is still in active development and this will likely be improved in future versions.

[87] L. P. Singer and L. R. Price, Rapid Bayesian position reconstruction for gravitational-wave transients, Phys. Rev. D **93**, 024013 (2016), arXiv:1508.03634 [gr-qc].

[88] L. P. Singer *et al.*, Going the Distance: Mapping Host Galaxies of LIGO and Virgo Sources in Three Dimensions Using Local Cosmography and Targeted Follow-up, Astrophys. J. Lett. **829**, L15 (2016), arXiv:1603.07333 [astro-ph.HE].

[89] C. García-Quirós, M. Colleoni, S. Husa, H. Estellés, G. Pratten, A. Ramos-Buades, M. Mateu-Lucena, and R. Jaume, Multimode frequency-domain model for the gravitational wave signal from nonprecessing black-hole binaries, Physical Review D **102**, 10.1103/phys

revd.102.064002 (2020).

[90] L. S. Collaboration and V. Collaboration, Noise curves for use in simulations pre-o4, DCC (2022).

[91] M. Prathaban, C. Hoy, and M. J. Williams, Leveraging simple-pe for efficient gravitational-wave parameter estimation via posterior repartitioning (2025), available at <https://zenodo.org/record/17776522>.

[92] A. G. Abac *et al.* (LIGO Scientific, VIRGO, KAGRA), GWTC-4.0: Updating the Gravitational-Wave Transient Catalog with Observations from the First Part of the Fourth LIGO-Virgo-KAGRA Observing Run, arXiv:2508.18082 (2025), arXiv:2508.18082 [gr-qc].

[93] A. Cabezas, A. Corenflos, J. Lao, and R. Louf, Blackjax: Composable Bayesian inference in JAX (2024), arXiv:2402.10797 [cs.MS].

[94] K. W. k. Wong, M. Gabré, and D. Foreman-Mackey, flowMC: Normalizing flow enhanced sampling package for probabilistic inference in JAX, *J. Open Source Softw.* **8**, 5021 (2023), arXiv:2211.06397 [astro-ph.IM].

[95] J. G. Albert, Jaxns: a high-performance nested sampling package based on jax (2020), arXiv:2012.15286 [astro-ph.IM].

[96] D. Yallup, N. Kroupa, and W. Handley, Nested slice sampling, in *Frontiers in Probabilistic Inference: Learning meets Sampling* (2025).

[97] M. Punturo *et al.*, The third generation of gravitational wave observatories and their science reach, *Class. Quant. Grav.* **27**, 084007 (2010).

[98] S. Hild *et al.*, Sensitivity Studies for Third-Generation Gravitational Wave Observatories, *Class. Quant. Grav.* **28**, 094013 (2011), arXiv:1012.0908 [gr-qc].

[99] M. Maggiore *et al.* (ET), Science Case for the Einstein Telescope, *JCAP* **03**, 050, arXiv:1912.02622 [astro-ph.CO].

[100] S. Babak, A. Petiteau, and M. Hewitson, LISA Sensitivity and SNR Calculations, arXiv:2108.01167 (2021), arXiv:2108.01167 [astro-ph.IM].

[101] M. Colpi *et al.* (LISA), LISA Definition Study Report, arXiv:2402.07571 (2024), arXiv:2402.07571 [astro-ph.CO].

[102] L. Kish, *Survey Sampling*, 3rd ed. (Wiley-Interscience, Oxford, England, 1995).

[103] C. Hoy and L. K. Nuttall, Bilby in space: Bayesian inference for transient gravitational-wave signals observed with lisa (2023), arXiv:2312.13039 [astro-ph.IM].

[104] A. Ramos-Buades, A. Buonanno, M. Khalil, and S. Ossokine, Effective-one-body multipolar waveforms for eccentric binary black holes with nonprecessing spins, *Phys. Rev. D* **105**, 044035 (2022), arXiv:2112.06952 [gr-qc].

[105] A. Gamboa *et al.*, Accurate waveforms for eccentric, aligned-spin binary black holes: The multipolar effective-one-body model seobnrv5ehm, *Phys. Rev. D* **112**, 044038 (2025), arXiv:2412.12823 [gr-qc].

[106] A. Nagar, R. Gamba, P. Rettegno, V. Fantini, and S. Bernuzzi, Effective-one-body waveform model for noncircularized, planar, coalescing black hole binaries: The importance of radiation reaction, *Phys. Rev. D* **110**, 084001 (2024), arXiv:2404.05288 [gr-qc].

[107] M. d. L. Planas, A. Ramos-Buades, C. García-Quirós, H. Estellés, S. Husa, and M. Haney, Time-domain phenomenological multipolar waveforms for aligned-spin binary black holes in elliptical orbits, arXiv:2503.13062 (2025), arXiv:2503.13062 [gr-qc].

[108] I. M. Romero-Shaw, C. Talbot, S. Biscoveanu, V. D'Emilio, G. Ashton, C. P. L. Berry, S. Coughlin, S. Galaudage, C. Hoy, M. Hübner, K. S. Phukon, M. Pitkin, M. Rizzo, N. Sarin, R. Smith, S. Stevenson, A. Vajpeyi, M. Arène, K. Athar, S. Banagiri, N. Bose, M. Carney, K. Chatzioannou, J. A. Clark, M. Colleoni, R. Cotesta, B. Edelman, H. Estellés, C. García-Quirós, A. Ghosh, R. Green, C.-J. Haster, S. Husa, D. Keitel, A. X. Kim, F. Hernandez-Vivanco, I. Magaña Hernandez, C. Karathanasis, P. D. Lasky, N. De Lillo, M. E. Lower, D. Macleod, M. Mateu-Lucena, A. Miller, M. Millhouse, S. Morisaki, S. H. Oh, S. Ossokine, E. Payne, J. Powell, G. Pratten, M. Pürer, A. Ramos-Buades, V. Raymond, E. Thrane, J. Veitch, D. Williams, M. J. Williams, and L. Xiao, Bayesian inference for compact binary coalescences with `jscp_bilby/scpi`: validation and application to the first ligo-virgo gravitational-wave transient catalogue, *Monthly Notices of the Royal Astronomical Society* **499**, 3295–3319 (2020).

[109] A. G. Samantha R Cook and D. B. Rubin, Validation of software for bayesian models using posterior quantiles, *Journal of Computational and Graphical Statistics* **15**, 675 (2006), <https://doi.org/10.1198/106186006X136976>.

[110] R. Abbott *et al.*, Gw190412: Observation of a binary-black-hole coalescence with asymmetric masses, *Physical Review D* **102**, 101103/physrevd.102.043015 (2020).

[111] R. Abbott *et al.*, Gw190521: A binary black hole merger with a total mass of  $150m_{\odot}$ , *Physical Review Letters* **125**, 10.1103/physrevlett.125.101102 (2020).

[112] A. G. Abac *et al.*, Gw231123: A binary black hole merger with total mass  $190\text{--}265 m_{\odot}$ , *The Astrophysical Journal Letters* **993**, L25 (2025).

[113] A. Begnoni, S. Anselmi, M. Pieroni, A. Renzi, and A. Ricciardone, Detectability and parameter estimation for einstein telescope configurations with `gwjulia` (2025), arXiv:2506.21530 [astro-ph.CO].

[114] M. J. Williams, M. Karamanis, Y. Luo, and U. Seljak, Validating sequential monte carlo for gravitational-wave inference, *Monthly Notices of the Royal Astronomical Society* **543**, 1479–1493 (2025).

[115] C. R. Harris *et al.*, Array programming with NumPy, *Nature* **585**, 357 (2020), arXiv:2006.10256 [cs.MS].

[116] C. Hoy and V. Raymond, PESummary: the code agnostic Parameter Estimation Summary page builder, *SoftwareX* **15**, 100765 (2021), arXiv:2006.06639 [astro-ph.IM].

[117] G. Ashton, M. Huebner, A. Legaspi, E. d'Emilio, M. Williams, C. Talbot, C. Hoy, P. Godwin, I. Romero-Shaw, S. Morisaki, S. Fairhurst, N. Sarin, R. Smith, S. Khan, P. Easter, S. Biscoveanu, M. Go, S. Galaudage, D. Jones, J. Lowry, M. E. Lower, M. Millhouse, O. Edy, E. Payne, and E. Thrane, Bilby: A user-friendly Bayesian inference library, <https://zenodo.org/records/14171800> (2024), version 2.4.0.

[118] W. Handley, anesthetic: nested sampling visualisation, *Journal of Open Source Software* **4**, 1414 (2019).

[119] J. D. Hunter, Matplotlib: A 2D Graphics Environment, *Comput. Sci. Eng.* **9**, 90 (2007).

[120] E. Hamilton, M. Colleoni, J. E. Thompson, C. Hoy, A. Heffernan, M. Kinnear, J. Valencia, F. A. R. Vidal, C. García-Quirós, S. Ghosh, L. London, M. Hanam, and S. Husa, Phenomxpn: An improved gravita-

tional wave model linking precessing inspirals and nr-calibrated merger-ringdown (2025), arXiv:2507.02604 [gr-qc].

[121] C. Hoy and V. Raymond, Pesummary: The code agnostic parameter estimation summary page builder, SoftwareX **15**, 100765 (2021).

[122] B. P. Abbott *et al.* (LIGO Scientific Collaboration and Virgo Collaboration), Gwtc-1: A gravitational-wave transient catalog of compact binary mergers observed by ligo and virgo during the first and second observing runs, Phys. Rev. X **9**, 031040 (2019).